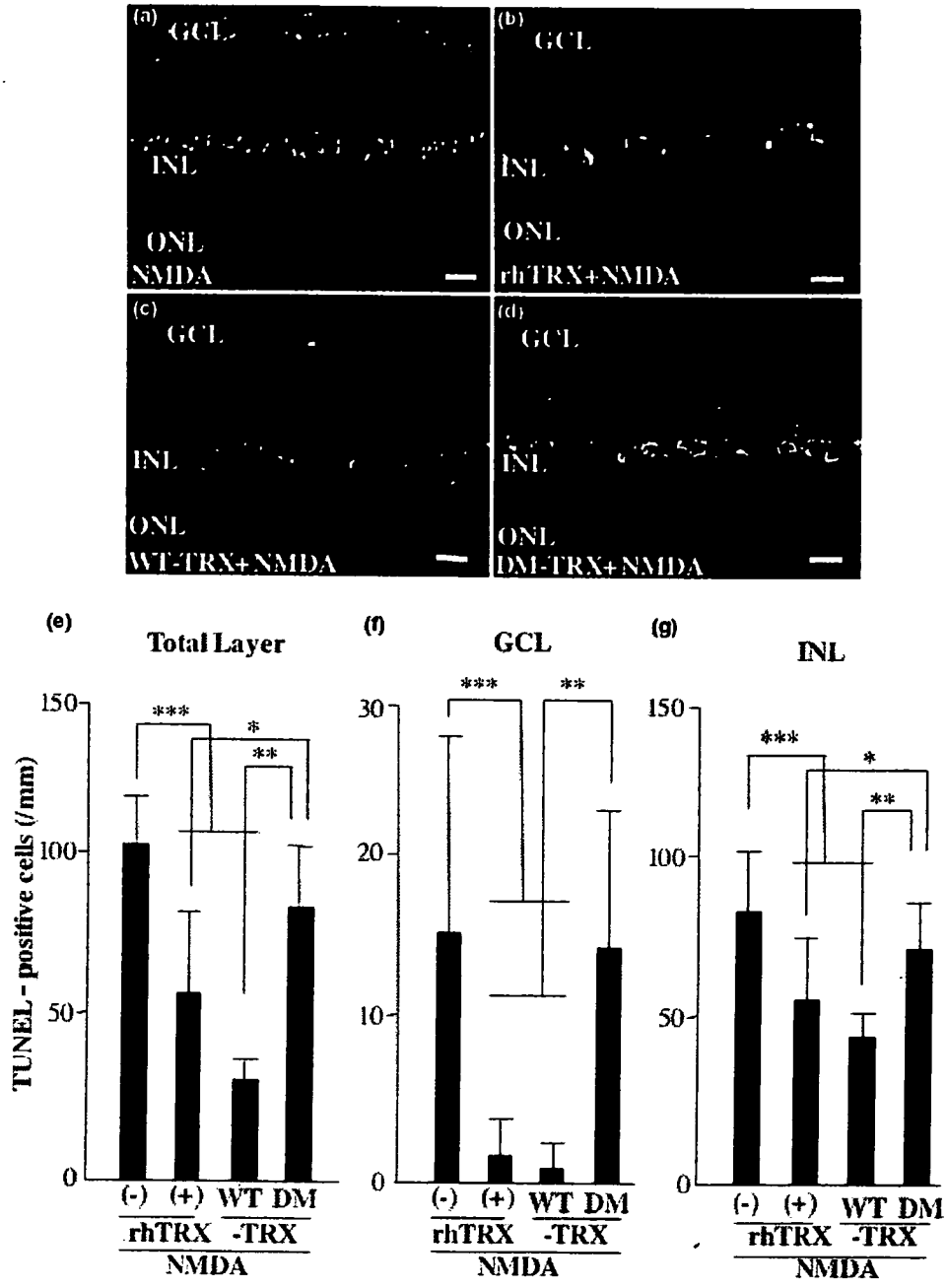

Fig. 3 Effect of thioredoxin (TRX) treatment on terminal deoxynucleotidyl transferase-mediated UTP nick-end labeling (TUNEL) in retinal sections 24 h after NMDA injection. Representative retinal specimens from eyes treated with NMDA and (a) vehicle, (b) 100 μg recombinant human (rh)TRX, (c) 100 μg wild-type (WT)-TRX or (d) 100 μg double-mutant (DM)-TRX. Green and red signals indicate TUNEL-positive cells and cell nuclei stained by propidium iodide, respectively (a–d). Scale bars, 50 μm. GCL, ganglion cell layer; INL, inner nuclear layer; ONL, outer nuclear layer. (e–g) Bar graphs show the mean ± SD densities of TUNEL-positive cells in sections from eyes treated with vehicle ($n = 9$), rhTRX ($n = 8$), WT-TRX ($n = 5$) and DM-TRX ($n = 5$) assessed in all retinal layers (e), in the GCL (f) and in the INL (g). The statistical significance of differences between groups was calculated by one-way ANOVA followed by Scheffe's post-hoc test. $^{*}p < 0.05$, $^{**}p < 0.01$ and $^{***}p < 0.001$.

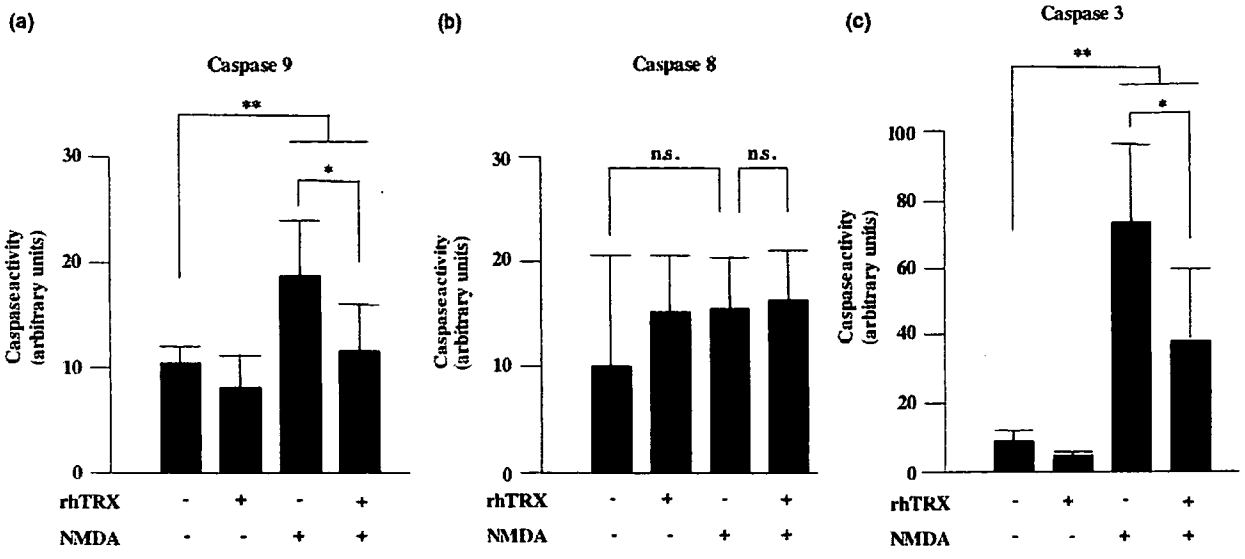

Fig. 4 Caspase activity in the retina after NMDA treatment. The activity of (a) caspase 9, (b) caspase 8 and (c) caspase 3 at 12, 12 and 18 h, respectively, after injection with NMDA and either vehicle or 100 μg recombinant human thioredoxin (rhTRX), as indicated. Bar graphs show the mean activity in arbitrary units (± SD; $n = 5$ in each group). The statistical significance of differences between groups was calculated by one-way ANOVA followed by Scheffe's post-hoc test. $^{*}p < 0.05$ and $^{**}p < 0.001$. n.s., not significant.

p-MKK4 (Fig. 7b) increased immediately after NMDA injection, and these kinases were maximally phosphorylated after 3 h. In eyes treated with rhTRX, WT-TRX, DM-TRX or vehicle simultaneously with NMDA injection (Figs 7a and b), the levels of p-MKK3/MKK6 and p-MKK4 in rhTRX-treated or WT-TRX-treated eyes were lower than those in vehicle-treated or DM-TRX-treated eyes after 3 h. These data indicate that TRX modulates signaling pathways upstream of p38 and JNK, and that the active site of TRX might be crucial in this activity.

Effects of thioredoxin on NMDA-induced oxidative stress

It has been proposed that oxidative stress is the trigger for various types of cellular response, including the activation of MAPKs and apoptotic signaling cascades. Therefore, we finally analysed the levels of oxidative stress induced in the retina by NMDA injection. Western blot and densitometric analysis showed that total levels of protein carbonylation in retinal samples gradually increased 6, 12 and 24 h after NMDA injection compared with the NMDA-untreated eyes (1.35-, 2.18- and 2.98-fold, respectively; Fig. 8a). At 18 h, retinal levels of protein carbonylation were markedly lower in rhTRX-treated compared with vehicle-treated eyes (0.55-fold; Fig. 8b). Interestingly, change of band intensities by rhTRX treatment was not uniform among proteins. As examples, the protein bands indicated by the upper and lower arrows in Fig. 8(b) decreased more than other bands in rhTRX-treated eyes (0.41- and 0.43-fold, respectively). Enzyme immunoassay revealed that the concentration of nitrotyrosine 18 h after NMDA injection was 113.1 ± 20.1 pmol/mg, which was significantly higher than the value in untreated eyes (57.7 ± 14.9 pmol/mg; $p < 0.001$; Fig. 8c). The NMDA-induced increase in nitrotyrosine concentration was significantly suppressed in the rhTRX-treated eyes (89.7 ± 4.3 pmol/mg; $p = 0.014$). There was no significant difference between the concentration of nitrotyrosine in vehicle-treated and rhTRX-treated eyes that had not been injected with NMDA. MDA was also significantly increased by NMDA treatment, reaching levels of 613.0 ± 204.2 pmol/mg compared with 168.0 ± 4.9 pmol/mg ($p < 0.001$) after 18 h (Fig. 8d). Considering protein carbonylation and nitrotyrosine, the NMDA-induced increase in MDA in the retina was significantly lower in rhTRX-treated eyes (360.7 ± 68.0 pmol/mg; $p = 0.019$). There was no significant difference between the MDA level in vehicle-treated and rhTRX-treated eyes that had not been injected with NMDA.

Discussion

We have shown that the intravitreous injection of TRX provided neuroprotection for rat retinal cells against NMDA-induced death. To date, effective cytoprotection by exogenously administered TRX protein has been shown in a variety of diseases (Nakamura *et al.* 2001; Hattori *et al.* 2004; Liu *et al.* 2004; Ichiki *et al.* 2005). However, the tissue distribution of TRX administered *in vivo* has not been studied extensively. In the current study, Alexa-labeled rhTRX injected into the vitreous cavity was detected in all retinal layers, including the retinal pigment epithelium, 1 h after

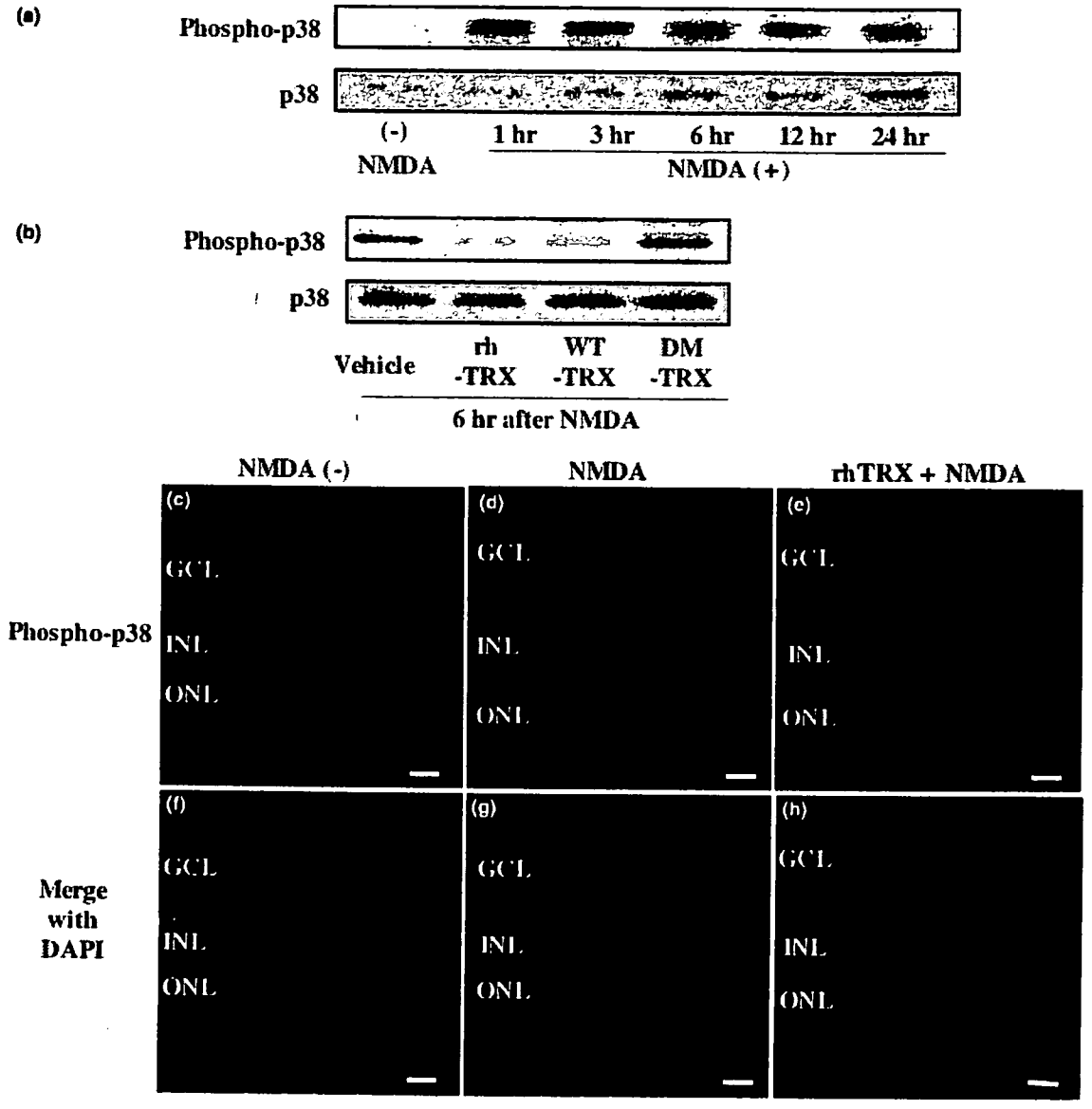

Fig. 5 Effect of thioredoxin (TRX) on NMDA-induced p38 kinase (p38) phosphorylation. Western blots showing (a) the time course of p38 phosphorylation after injection with 20 nmol NMDA and (b) the effect of TRX on p38 phosphorylation at 6 h after NMDA injection. Vehicle or 100 μg recombinant human (rh)TRX, wild-type (WT)-TRX or double-mutant (DM)-TRX was injected with NMDA. (c–h) Representative retinal sections labeled immunohistochemically for phospho (p)-p38 (c–e) or p-p38 merged with 4′,6-diamidino-2-phenylindole (DAPI) staining (f–h) from control eyes (c and f) or eyes treated with NMDA 6 h earlier, either with vehicle (d and g) or with rhTRX (e and h). Strong labeling for p-p38 is present in the ganglion cell layer (GCL) and inner nuclear layer (INL) in vehicle-treated eyes (d and g) and is reduced in rhTRX-treated eyes (e and h). Scale bars, 50 μm. ONL, outer nuclear layer.

injection and up to 24 h later (Fig. 1). Surprisingly, TRX labeling in the outer retina (i.e. the rod inner segment, rod outer segment and retinal pigment epithelium) increased over time (Fig. 1; 24 h), suggesting that some active-transport system might be involved in its accumulation. This is in line with a previous report showing the cytoprotective effects of TRX injected intravitreally in a model of light-induced photoreceptor cell damage (Tanito *et al.* 2002a). Although the underlying mechanism is to be further investigated, this suggests a high bioavailability of TRX in the retinal tissue.

Retrograde labeling showed that the density of RGCs was significantly higher in eyes treated intravitreally with rhTRX simultaneously with NMDA injection than in those treated with saline (Fig. 2), suggesting that TRX inhibited the

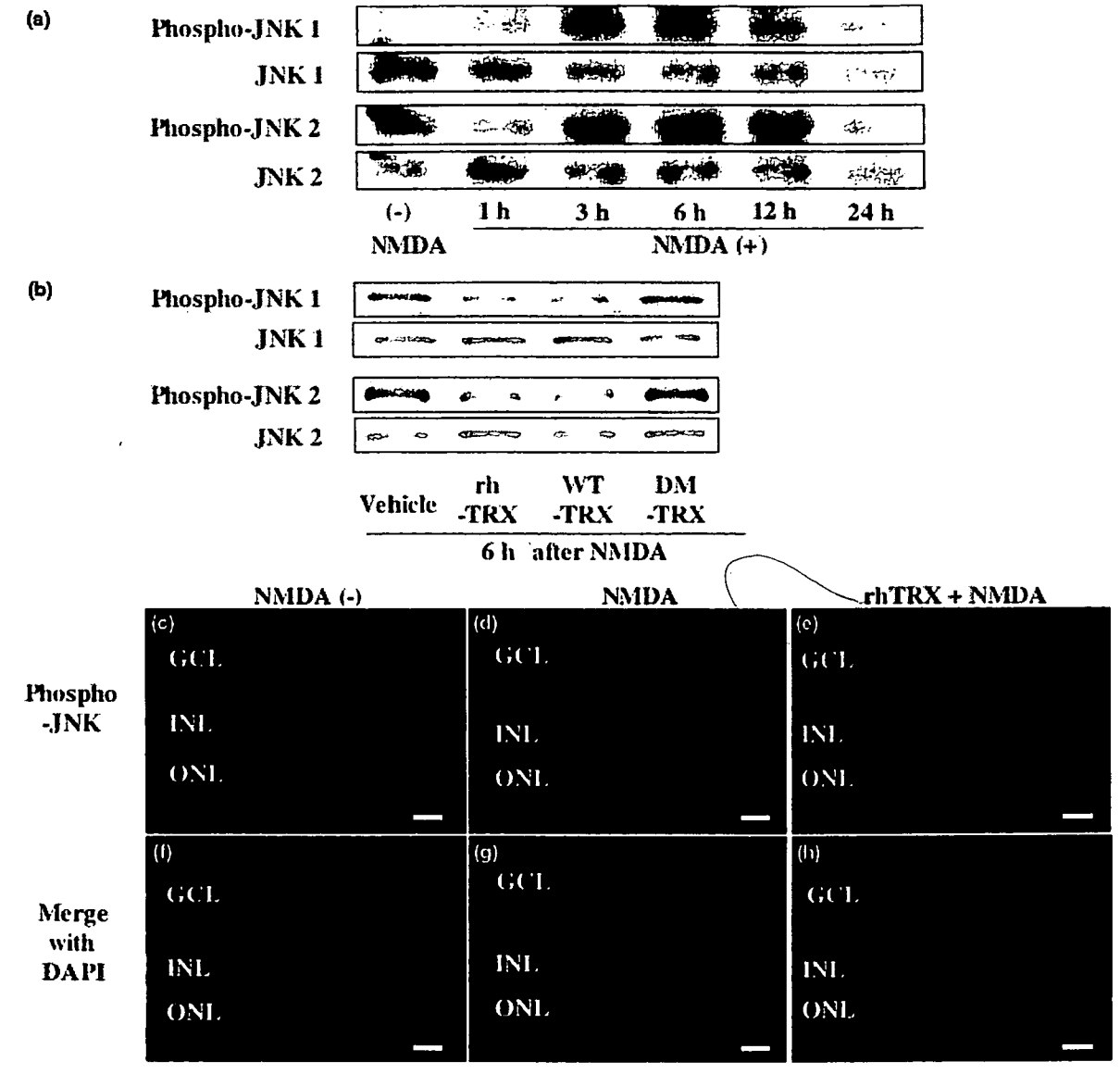

Fig. 6 Effect of thioredoxin (TRX) on NMDA-induced c-Jun N-terminal kinase (JNK) phosphorylation. Western blots showing (a) the time course of JNK phosphorylation after injection with 20 nmol NMDA and (b) the effect of TRX on JNK phosphorylation at 6 h after NMDA injection. Vehicle or 100 μg recombinant human (rh)TRX, wild-type (WT)-TRX or double-mutant (DM)-TRX was injected with NMDA. Representative retinal sections labeled immunohistochemically for phospho (p)-JNK (c–e) or p-JNK merged with 4′,6-diamidino-2-phenylindole (DAPI) staining (f–h) from control eyes (c and f) or eyes treated with NMDA 6 h earlier, either with vehicle (d and g) or with rhTRX (e and h). Strong labeling for p-JNK is present in the ganglion cell layer (GCL) in vehicle-treated eyes (d and g) and is lower in rhTRX-treated eyes (e and h). Scale bars, 50 μm. INL, inner nuclear layer; ONL, outer nuclear layer.

NMDA-induced loss of RGCs. After NMDA injection, there were significantly fewer TUNEL-positive cells in both the GCL and INL in rhTRX-treated and WT-TRX-treated eyes than in saline-treated and DM-TRX-treated eyes (Fig. 3). This provided additional evidence of the antiapoptotic effect of TRX on NMDA-induced neurotoxicity and suggested that the conserved cysteine residues in the redox-active site in TRX might have an important role in this process. These results support the evidence of previous studies that demonstrated a protective effect of TRX in neuronal cell apoptosis, both *in vivo* (Tanito *et al.* 2002a; Chiueh *et al.* 2005) and *in vitro* (Bai *et al.* 2002). Actually, NMDA receptor itself contains several cysteines in the structure and has some sensitivity on the thiol-mediated redox regulation function (Lipton *et al.* 2002; Herin and Aizenman 2004). The possibility that TRX may modulate the ligand binding and

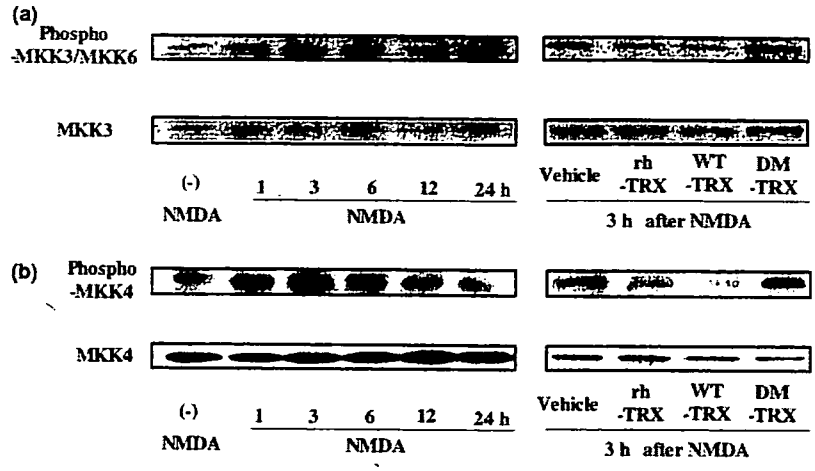

Fig. 7 Effect of thioredoxin (TRX) on NMDA-induced MAPK kinase (MKK) phosphorylation. Western blots showing the phosphorylation of MKK3/MKK6 (a) and MKK4 (b) in retinal samples. The left panels show time courses for phosphorylation after injection with 20 nmol NMDA. The right panels show the effects of injecting vehicle or 100 μg recombinant human (rh)TRX, wild-type (WT)-TRX or double-mutant (DM)-TRX with NMDA. Samples were collected 3 h after the injection.

signal transduction by redox regulation is to be clarified in the future.

The marked activation of caspase 9 and 3, but not caspase 8, in the retina by NMDA (Fig. 4) suggested that it induces apoptosis via the mitochondrial pathway, as has been previously suggested (Budd *et al.* 2000). This NMDA-induced activation of caspase 9 and 3 was significantly inhibited by rhTRX. A previous study showed that this apoptotic pathway could be inhibited by the endogenous mitochondrial form of TRX, TRX-2 (Tanaka *et al.* 2002). Our results showed that exogenous TRX-1 could also inhibit the mitochondrial apoptotic pathway; thus, to elucidate the mechanism involved, we examined the effect of TRX on molecules implicated in upstream signaling in this pathway.

Several lines of evidence have suggested that the mitochondrial apoptotic pathway in neurons is specifically regulated by the MAPKs p38 and JNKs (Mielke and Herdegen 2000; Bossy-Wetzel *et al.* 2004). In models of NMDA-induced retinal damage, possible links between the activation of p38 and JNKs, and apoptosis in RGCs, have been reported recently (Manabe and Lipton 2003; Munemasa *et al.* 2005). We used western blot analysis and immunohistochemistry to demonstrate that the phosphorylation of both p38 and JNKs increased after NMDA injection in whole retinal samples, and that these phosphorylation events were specifically localized in the GCL (Figs 5 and 6), in agreement with previous reports. These increases in phosphorylation were clearly suppressed by rhTRX and WT-TRX but not by DM-TRX (Figs 5 and 6). The kinases upstream of p-38 and JNKs have not been extensively studied in NMDA-induced apoptosis in RGCs. Using western blot analysis, we showed that the phosphorylation of both MKK3/MKK6 and MKK4 increased after NMDA injection, and at earlier time points than the phosphorylation of p38 and JNKs (Fig. 7), indicating that the activation of specific MKKs and MAPKs is involved in the signal-transduction pathway leading to apoptosis in RGCs. This increase in MKK phosphorylation was also clearly suppressed by rhTRX and WT-TRX but not DM-TRX (Fig. 7). Thus, our findings strongly suggest that the suppression of these signaling cascades, specific to NMDA-induced apoptosis, is involved in the cytoprotective mechanism of TRX and that its redox-active region is crucial for its effect on these kinase cascades.

It is well established that various types of oxidative stress trigger the activation of MAPK cascades (Choi *et al.* 2004) and, subsequently, the mitochondrial apoptosis pathway (Ueda *et al.* 2002). In the current study, all the oxidative-stress markers analysed, including protein carbonylation, tyrosine nitrosylation and lipid peroxidation, were enhanced by injecting NMDA into retinal tissue (Fig. 8). These increases in oxidative-stress markers were clearly suppressed by TRX (Fig. 8), suggesting that it effectively attenuated the oxidative stress induced by NMDA. Interestingly, some proteins were better protected by TRX from the carbonylation than others (Fig. 8), suggesting a presence of specific target proteins for neuroprotection by TRX, but this needs to be tested. TRX has been reported to scavenge hydroxyl radicals or singlet oxygen by itself (Das and Das 2000) and to eliminate hydrogen peroxide in cooperation with peroxiredoxins (Chae *et al.* 1994); the latter are also abundantly expressed in retinal tissue, including the inner retina (Tanito *et al.* 2005b). Peroxynitrite ($ONOO^-$) is produced by the accumulation of superoxides and nitric oxides, and causes lipid peroxidation, mitochondrial dysfunction and, eventually, cell death (Coyle and Puttfarcken 1993). Accordingly, the elimination of reactive oxygen species in the extracellular space or at the cellular membrane, and inhibition of subsequent reactive nitrogen species and lipid peroxide formation, might be involved in the antioxidative effects of TRX in this study. An imbalance in the extracellular redox status changes the thiol content at the external surface of the cell membrane, and affects the intracellular redox status of both the TRX and glutathione systems; these changes are sensed by p38 (Filomeni *et al.* 2003). In the intracellular

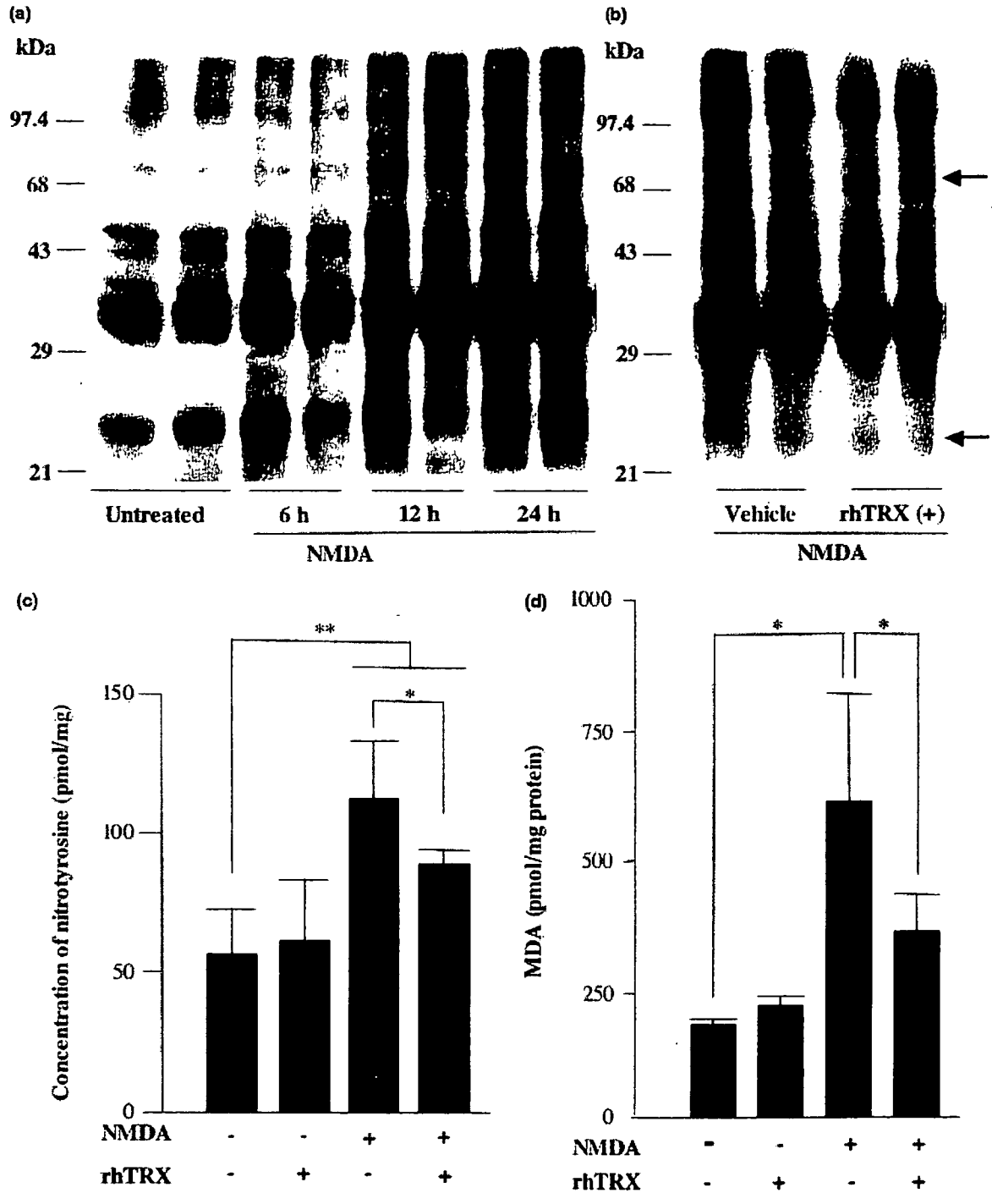

Fig. 8 Effects of thioredoxin (TRX) on NMDA-induced markers of oxidative stress. Western blots showing (a) the time course of protein carbonylation after injection with 20 nmol NMDA and (b) the effect of injecting vehicle or 100 μg recombinant human (rh)TRX with NMDA. Samples were collected 18 h after the injection. (c) Enzyme immunoassay for nitrotyrosine and (d) the measurement of malondialdehyde in retinal samples collected 18 h after injection with NMDA with vehicle or 100 μg rhTRX, as indicated in the figure. The results are expressed as means ± SD ($n = 6$ and 5 in c and d, respectively). The statistical significance of differences between groups was calculated by one-way ANOVA followed by Scheffe's post-hoc test. $^{*}p < 0.05$ and $^{**}p < 0.001$.

space, TRX directly binds to the apoptosis signal-regulating kinase-1, which is an MKK kinase that activates p38 and JNK pathways, and so inhibits apoptosis signal-regulating kinase-1-dependent apoptosis (Saitoh *et al.* 1998). Our recent data suggested that exogenous TRX might be taken up into the intracellular space (Kondo *et al.*, unpublished data). In view of this, we can speculate that the maintenance of the extracellular redox status and/or the direct regulation of an MAPK cascade molecule might be involved in the cytoprotective effect of exogenously administrated TRX but this remains to be tested. The possible relation between decrease of intracellular glutathione level and glutamate-induced neurotoxicity (Murphy *et al.* 1989), and between increase of extracellular glutathione level and neuroprotection against NMDA-induced neurotoxicity (Levy *et al.* 1991) was reported *in vitro*. However, in contrast to TRX, modulatory effects against the NMDA-induced MAPK-apoptosis pathway and bioavailability of glutathione in retinal tissue are still unclear *in vivo*.

Glutamate receptors are categorized into two main classes: ionotropic and metabotropic. Ionotropic glutamate receptors are further classified into NMDA- and non-NMDA-(α-amino-3-hydroxy-5-methyl-4-isoxazolepropionic acid and kainic acid) type receptors. RGCs and amacrine cells possess not only NMDA-type receptors but also α-amino-3-hydroxy-5-methyl-4-isoxazolepropionic acid/kainic acid-type receptors and metabotropic glutamate receptors, and bipolar cells also possess α-amino-3-hydroxy-5-methyl-4-isoxazolepropionic acid/kainic acid-type receptors and metabotropic glutamate receptors (Thoreson and Witkovsky 1999). As NMDA is not normally present in animal systems, we additionally tested the effect of TRX against neurotoxicity induced by glutamate, a natural agonist of both classes of glutamate receptors. At 12 h after a 2-μL (400 nmol) L-glutamate injection, TUNEL-positive cells were observed in GCL and INL, and the number of TUNEL-positive cells in these retinal layers was significantly less in TRX-treated than in vehicle-treated eyes (59.3 ± 12.4 and 21 ± 3.7 cells/mm, respectively, in GCL, $p = 0.025$; 72.3 ± 12.4 and 34.5 ± 7.1 cells/mm, respectively, in INL, $p = 0.021$). At the same time point after L-glutamate injection, caspase 3 activity in retina was significantly increased compared with that in un-injected retina (2.64-fold and $p < 0.001$), whereas the increase was less remarkable in rhTRX-treated retina (1.35-fold and $p = 0.413$ in comparison with un-injected retina; $p = 0.003$ in comparison with vehicle-treated retina). These results support a previous report that NMDA closely mimicked glutamate-induced neurotoxicity (Schori *et al.* 2001). Taken together, TRX is likely to be protective against glutamate-induced neurotoxicity in natural animal systems.

Expression of TRX is reported in the nerve and photoreceptor cells from developing and mature rat retinas (Hansson *et al.* 1989). We previously reported that endogenous TRX was expressed throughout the retinal layers and was up-regulated by oxidative stresses such as photo-oxidative stress in mouse, indicating that the increase of TRX level in retina is likely to be a defence mechanism against retinal pathology (Tanito *et al.* 2005a). The use of TRX inducers, such as sulforaphane and geranylgeranylacetone, was an effective and safe way to up-regulate TRX *in vivo* (Tanito *et al.* 2005a,b). As NMDA-induced neuronal cell death is well established as a useful model, which is relevant to the pathogenesis of many degenerative diseases, our previous studies and the results presented here suggest novel approaches to the development of new therapies for these diseases.

In conclusion, the intravitreous injection of TRX effectively attenuated NMDA-induced retinal cell damage. The inhibition of oxidative stress and the modulation of signaling cascades, including MKKs, MAPKs and the mitochondrial apoptotic pathway, likely to act downstream of oxidative stress, were all implicated in the cytoprotective mechanism of TRX.

Acknowledgements

The authors thank Mrs A. Abe for her excellent technical assistance, and Drs Y. Hoshino, T. Nakamura, H. Masutani and A. Takano for valuable discussions. This work was supported by a Grant-in-Aid for Scientific Research from the Japanese Ministry of Education, Science, Sports and Culture, and from the Ministry of Health and Welfare of Japan.

References

Bai J., Nakamura H., Hattori I., Tanito M. and Yodoi J. (2002) Thioredoxin suppresses 1-methyl-4-phenylpyridinium-induced neurotoxicity in rat PC12 cells. *Neurosci. Lett.* **321**, 81–84.

Bai J., Nakamura H., Kwon Y. W. *et al.* (2003) Critical roles of thioredoxin in nerve growth factor-mediated signal transduction and neurite outgrowth in PC12 cells. *J. Neurosci.* **23**, 503–509.

Bonfoco E., Krainc D., Ankarcrona M., Nicotera P. and Lipton S. A. (1995) Apoptosis and necrosis: two distinct events induced, respectively, by mild and intense insults with *N*-methyl-D-aspartate or nitric oxide/superoxide in cortical cell cultures. *Proc. Natl Acad. Sci. USA* **92**, 7162–7166.

Bossy-Wetzel E., Talantova M. V., Lee W. D. *et al.* (2004) Crosstalk between nitric oxide and zinc pathways to neuronal cell death involving mitochondrial dysfunction and p38-activated K^+ channels. *Neuron* **41**, 351–365.

Brandstatter J. H., Hartveit E., Sassoe-Pognetto M. and Wassle H. (1994) Expression of NMDA and high-affinity kainate receptor subunit mRNAs in the adult rat retina. *Eur. J. Neurosci.* **6**, 1100–1112.

Budd S. L., Tenneti L., Lishnak T. and Lipton S. A. (2000) Mitochondrial and extramitochondrial apoptotic signaling pathways in cerebrocortical neurons. *Proc. Natl Acad. Sci. USA* **97**, 6161–6166.

Cao G., Minami M., Pei W., Yan C., Chen D., O'Horo C., Graham S. H. and Chen J. (2001) Intracellular Bax translocation after transient cerebral ischemia: implications for a role of the mitochondrial apoptotic signaling pathway in ischemic neuronal death. *J. Cereb. Blood Flow Metab.* **21**, 321–333.

Chae H. Z., Chung S. J. and Rhee S. G. (1994) Thioredoxin-dependent peroxide reductase from yeast. *J. Biol. Chem.* **269**, 27 670–27 678.

Chiueh C. C., Andoh T. and Chock P. B. (2005) Induction of thioredoxin and mitochondrial survival proteins mediates preconditioning-induced cardioprotection and neuroprotection. *Ann. NY Acad. Sci.* **1042**, 403–418.

Choi W. S., Eom D. S., Han B. S., Kim W. K., Han B. H., Choi E. J., Oh T. H., Markelonis G. J., Cho J. W. and Oh Y. J. (2004) Phosphorylation of p38 MAPK induced by oxidative stress is linked to activation of both caspase-8- and -9-mediated apoptotic pathways in dopaminergic neurons. *J. Biol. Chem.* **279**, 20 451–20 460.

Coyle J. T. and Puttfarcken P. (1993) Oxidative stress, glutamate, and neurodegenerative disorders. *Science* **262**, 689–695.

Das K. C. and Das C. K. (2000) Thioredoxin, a singlet oxygen quencher and hydroxyl radical scavenger: redox independent functions. *Biochem. Biophys. Res. Commun.* **277**, 443–447.

El-Remessy A. B., Khalil I. E., Matragoon S., Abou-Mohamed G., Tsai N. J., Roon P., Caldwell R. B., Caldwell R. W., Green K. and Liou G. I. (2003) Neuroprotective effect of (-)Delta9-tetrahydrocannabinol and cannabidiol in *N*-methyl-D-aspartate-induced retinal neurotoxicity: involvement of peroxynitrite. *Am. J. Pathol.* **163**, 1997–2008.

Filomeni G., Rotilio G. and Ciriolo M. R. (2003) Glutathione disulfide induces apoptosis in U937 cells by a redox-mediated p38 MAP kinase pathway. *FASEB J.* **17**, 64–66.

Hansson H. A., Holmgren A., Norstedt G. and Rozell B. (1989) Changes in the distribution of insulin-like growth factor I, thioredoxin, thioredoxin reductase and ribonucleotide reductase during the development of the retina. *Exp. Eye Res.* **48**, 411–420.

Hartwick A. T., Lalonde M. R., Barnes S. and Baldridge W. H. (2004) Adenosine A1-receptor modulation of glutamate-induced calcium influx in rat retinal ganglion cells. *Invest. Ophthalmol. Vis. Sci.* **45**, 3740–3748.

Hattori I., Takagi Y., Nakamura H., Nozaki K., Bai J., Kondo N., Sugino T., Nishimura M., Hashimoto N. and Yodoi J. (2004) Intravenous administration of thioredoxin decreases brain damage following transient focal cerebral ischemia in mice. *Antioxid. Redox Signal* **6**, 81–87.

Herin G. A. and Aizenman E. (2004) Amino terminal domain regulation of NMDA receptor function. *Eur. J. Pharmacol.* **500**, 101–111.

Holmgren A. (1985) Thioredoxin. *Annu. Rev. Biochem.* **54**, 237–271.

Ichiki H., Hoshino T., Kinoshita T., Imaoka H., Kato S., Inoue H., Nakamura H., Yodoi J., Young H. A. and Aizawa H. (2005) Thioredoxin suppresses airway hyperresponsiveness and airway inflammation in asthma. *Biochem. Biophys. Res. Commun.* **334**, 1141–1148.

Inomata Y., Hirata A., Yonemura N., Koga T., Kido N. and Tanihara H. (2003a) Neuroprotective effects of interleukin-6 on NMDA-induced rat retinal damage. *Biochem. Biophys. Res. Commun.* **302**, 226–232.

Inomata Y., Hirata A., Koga T., Kimura A., Singh D. P., Shinohara T. and Tanihara H. (2003b) Lens epithelium-derived growth factor: neuroprotection on rat retinal damage induced by *N*-methyl-D-aspartate. *Brain Res.* **991**, 163–170.

Kondo N., Ishii Y., Kwon Y. W., Tanito M., Horita H., Nishinaka Y., Nakamura H. and Yodoi J. (2004) Redox-sensing release of human thioredoxin from T lymphocytes with negative feedback loops. *J. Immunol.* **172**, 442–448.

Lam T. T., Abler A. S., Kwong J. M. and Tso M. O. (1999) *N*-methyl-D-aspartate (NMDA)-induced apoptosis in rat retina. *Invest. Ophthalmol. Vis. Sci.* **40**, 2391–2397.

Levin L. A. and Louhab A. (1996) Apoptosis of retinal ganglion cells in anterior ischemic optic neuropathy. *Arch. Ophthalmol.* **114**, 488–491.

Levy D. I., Sucher N. J. and Lipton S. A. (1991) Glutathione prevents N-methyl-D-aspartate receptor-mediated neurotoxicity. *Neuroreport* **2**, 345–347.

Lipton S. A., Choi Y. B., Takahashi H., Zhang D., Li W., Godzik A. and Bankston L. A. (2002) Cysteine regulation of protein function – as exemplified by NMDA-receptor modulation. *Trends Neurosci.* **25**, 474–480.

Liu W., Nakamura H., Shioji K., Tanito M., Oka S., Ahsan M. K., Son A., Ishii Y., Kishimoto C. and Yodoi J. (2004) Thioredoxin-1 ameliorates myosin-induced autoimmune myocarditis by suppressing chemokine expressions and leukocyte chemotaxis in mice. *Circulation* **110**, 1276–1283.

Manabe S. and Lipton S. A. (2003) Divergent NMDA signals leading to proapoptotic and antiapoptotic pathways in the rat retina. *Invest. Ophthalmol. Vis. Sci.* **44**, 385–392.

Masutani H., Ueda S. and Yodoi J. (2005) The thioredoxin system in retroviral infection and apoptosis. *Cell Death Differ.* **12**, 991–998.

Mielke K. and Herdegen T. (2000) JNK and p38 stresskinases — degenerative effectors of signal-transduction-cascades in the nervous system. *Prog. Neurobiol.* **61**, 45–60.

Mitsui A., Hirakawa T. and Yodoi J. (1992) Reactive oxygen-reducing and protein-refolding activities of adult T cell leukemia-derived factor/human thioredoxin. *Biochem. Biophys. Res. Commun.* **186**, 1220–1226.

Munemasa Y., Ohtani-Kaneko R., Kitaoka Y. *et al.* (2005) Contribution of mitogen-activated protein kinases to NMDA-induced neurotoxicity in the rat retina. *Brain Res.* **1044**, 227–240.

Murphy T. H., Miyamoto M., Sastre A., Schnaar R. L. and Coyle J. T. (1989) Glutamate toxicity in a neuronal cell line involves inhibition of cystine transport leading to oxidative stress. *Neuron* **2**, 1547–1558.

Nakamura H., Nakamura K. and Yodoi J. (1997) Redox regulation of cellular activation. *Annu. Rev. Immunol.* **15**, 351–369.

Nakamura H., Herzenberg L. A., Bai J., Araya S., Kondo N., Nishinaka Y., Herzenberg L. A. and Yodoi J. (2001) Circulating thioredoxin suppresses lipopolysaccharide-induced neutrophil chemotaxis. *Proc. Natl Acad. Sci. USA* **98**, 15 143–15 148.

Rosenbaum D. M., Rosenbaum P. S., Gupta H., Singh M., Aggarwal A., Hall D. H., Roth S. and Kessler J. A. (1998) The role of the p53 protein in the selective vulnerability of the inner retina to transient ischemia. *Invest. Ophthalmol. Vis. Sci.* **39**, 2132–2139.

Saitoh M., Nishitoh H., Fujii M., Takeda K., Tobiume K., Sawada Y., Kawabata M., Miyazono K. and Ichijo H. (1998) Mammalian thioredoxin is a direct inhibitor of apoptosis signal-regulating kinase (ASK) 1. *EMBO J.* **17**, 2596–2606.

Schori H., Kipnis J., Yoles E., WoldeMussie E., Ruiz G., Wheeler L. A. and Schwartz M. (2001) Vaccination for protection of retinal ganglion cells against death from glutamate cytotoxicity and ocular hypertension: implications for glaucoma. *Proc. Natl Acad. Sci. USA* **98**, 3398–3403.

Schwarcz R. and Coyle J. T. (1977) Kainic acid: neurotoxic effects after intraocular injection. *Invest. Ophthalmol. Vis. Sci.* **16**, 141–148.

Shibuki H., Katai N., Kuroiwa S., Kurokawa T., Yodoi J. and Yoshimura N. (1998) Protective effect of adult T-cell leukemia-derived factor on retinal ischemia-reperfusion injury in the rat. *Invest. Ophthalmol. Vis. Sci.* **39**, 1470–1477.

Siliprandi R., Canella R., Carmignoto G., Schiavo N., Zanellato A., Zanoni R. and Vantini G. (1992) *N*-methyl-D-aspartate-induced neurotoxicity in the adult rat retina. *Vis. Neurosci.* **8**, 567–573.

Sucher N. J., Lipton S. A. and Dreyer E. B. (1997) Molecular basis of glutamate toxicity in retinal ganglion cells. *Vision Res.* **37**, 3483–3493.

Tagaya Y., Maeda Y., Mitsui A. *et al.* (1989) ATL-derived factor (ADF), an IL-2 receptor/Tac inducer homologous to thioredoxin; possible involvement of dithiol-reduction in the IL-2 receptor induction. *EMBO J.* **8**, 757–764.

Takagi Y., Mitsui A., Nishiyama A., Nozaki K., Sono H., Gon Y., Hashimoto N. and Yodoi J. (1999) Overexpression of thioredoxin in transgenic mice attenuates focal ischemic brain damage. *Proc. Natl Acad. Sci.* **96**, 4131–4134.

Tanaka T., Hosoi F., Yamaguchi-Iwai Y. *et al.* (2002) Thioredoxin-2 (TRX-2) is an essential gene regulating mitochondria-dependent apoptosis. *EMBO J.* **21**, 1695–1703.

Tanito M., Masutani H., Nakamura H., Ohira A. and Yodoi J. (2002a) Cytoprotective effect of thioredoxin against retinal photic injury in mice. *Invest. Ophthalmol. Vis. Sci.* **43**, 1162–1167.

Tanito M., Masutani H., Nakamura H., Oka S., Ohira A. and Yodoi J. (2002b) Attenuation of retinal photooxidative damage in thioredoxin transgenic mice. *Neurosci. Lett.* **326**, 142–146.

Tanito M., Nishiyama A., Tanaka T., Masutani H., Nakamura H., Yodoi J. and Ohira A. (2002c) Change of redox status and modulation by thiol replenishment in retinal photooxidative damage. *Invest. Ophthalmol. Vis. Sci.* **43**, 2392–2400.

Tanito M., Masutani H., Kim Y. C., Nishikawa M., Ohira A. and Yodoi J. (2005a) Sulforaphane induces thioredoxin through the antioxidant-responsive element and attenuates retinal light damage in mice. *Invest. Ophthalmol. Vis. Sci.* **46**, 979–987.

Tanito M., Kwon Y. W., Kondo N., Bai J., Masutani H., Nakamura H., Fujii J., Ohira A. and Yodoi J. (2005b) Cytoprotective effects of geranylgeranylacetone against retinal photooxidative damage. *J. Neurosci.* **25**, 2396–2404.

Thoreson W. B. and Witkovsky P. (1999) Glutamate receptors and circuits in the vertebrate retina. *Prog. Retin. Eye Res.* **18**, 765–810.

Ueda S., Nakamura H., Masutani H., Sasada T., Yonehara S., Takabayashi A., Yamaoka Y. and Yodoi J. (1998) Redox regulation of caspase-3(-like) protease activity: regulatory roles of thioredoxin and cytochrome c. *J. Immunol.* **161**, 6689–6695.

Ueda S., Masutani H., Nakamura H., Tanaka T., Ueno M. and Yodoi J. (2002) Redox control of cell death. *Antioxid. Redox Signal* **4**, 405–414.

Wehrwein E., Thompson S. A., Coulibaly S. F., Linn D. M. and Linn C. L. (2004) Acetylcholine protection of adult pig retinal ganglion cells from glutamate-induced excitotoxicity. *Invest. Ophthalmol. Vis. Sci.* **45**, 1531–1543.

Yodoi J. and Uchiyama T. (1992) Diseases associated with HTLV-I: virus, IL-2 receptor dysregulation and redox regulation. *Immunol. Today* **13**, 405–411.

Molecular Vision 2006; 12:977-82 <http://www.molvis.org/molvis/v12/a109/>
Received 22 December 2005 | Accepted 16 June 2006 | Published 17 August 2006

Elevated neprilysin activity in vitreous of patients with proliferative diabetic retinopathy

Hideaki Hara,[1] Kentaro Oh-hashi,[2] Shinji Yoneda,[3] Masamitsu Shimazawa,[1] Masaru Inatani,[4] Hidenobu Tanihara,[4] Kazutoshi Kiuchi[2]

[1]Department of Biofunctional Molecules, Gifu Pharmaceutical University, 5-6-1 Mitahora-higashi, Gifu, [2]Department of Biomolecular Science, Faculty of Engineering, Gifu University, 1-1 Yanagido, Gifu, [3]Research and Development Center, Santen Pharmaceutical Co. Ltd., 8916-16 Takayama-cho, Ikoma, [4]Department of Ophthalmology and Visual Science, Kumamoto University Graduate School of Medical Sciences, 1-1-1 Honjo, Kumamoto, Japan

Purpose: Diabetic retinopathy (DR) is the leading cause of blindness in the industrialized world. Hyperglycemia induces retinal hypoxia, which upregulates a range of vasoactive factors that may lead to macular edema and/or angiogenesis, and hence potentially to sight-threatening retinopathy. The control of signal-peptide activity by cell-surface proteases is one of the main factors regulating the development and behavior of organisms. In mammals, neprilysin is known to play a key role in these processes, and its inactivation can initiate cellular disorganization. Neprilysin is a rate-limiting peptidase involved in the physiological degradation of amyloid β (Aβ) in the brain. In this study, we measured both the enzymatic activity of neprilysin and the concentration of Aβ in patients with proliferative DR (as compared to their levels in patients with macular hole), and we analyzed their association.

Methods: In vitreous samples collected from patients who underwent vitrectomy, an HPLC-fluorometric system (recently established by us), and sensitive and specific enzyme-linked immunosorbent assays were used to determine the enzymatic activity of neprilysin and the concentration of Aβ.

Results: By comparison with the levels in the control (macular-hole) patients, there was a significant increase in neprilysin activity level and a significant decrease in Aβ level in proliferative DR patients. There was a significant inverse correlation between neprilysin and Aβ among all subjects.

Conclusions: Neprilysin activity and Aβ concentrations displayed converse changes in patients with proliferative DR.

Diabetic retinopathy (DR) is the leading cause of acquired blindness among young adults, and studies have shown that it is the hyperglycemia itself that initiates its development [1]. In the pathogenesis of retinopathy in diabetes, certain cells (retinal microvascular endothelial, Müller, and ganglion cells and pericytes) are lost selectively via apoptosis before any other histopathology is detectable and before any loss of vision is evident [2,3].

Alzheimer's disease (AD) is characterized by the accumulation of amyloid β peptide (Aβ) in the brain. Aβ is constitutively produced by proteolysis of β-amyloid precursor protein (APP) [4,5]. The pathological formation of amyloid plaques is thought to be the primary force driving the pathogenesis of Alzheimer's disease. Hence, much attention has been focused on the production of Aβ. Neprilysin (variously known as neutrophil cluster-differentiation antigen 10 (CD10), neuronal endopeptidase 24-11, or enkephalinase) is considered the most important enzyme for Aβ degradation in the brain [6,7]. Recently, genetic approaches using neprilysin-deficient mice have demonstrated the ability of neprilysin to cleave endogenous Aβ [8,9]. Moreover, a decline in neprilysin levels has been found in the brain in patients with early-stage sporadic AD [10], suggesting critical roles for reduced neprilysin activity in the incipient process of Aβ accumulation.

The prevalence of both Alzheimer disease and type 2 diabetes increases with age, and both have genetic components [11-16], raising the possibilitity that patients with Alzheimer disease may be more vulnerable to type 2 diabetes and raising the possibility of a linkage between the processes responsible for the loss of brain cells and the loss of β-cells in these diseases [17]. It has been reported that diabetes-related mitochondrial dysfunction is exacerbated by aging and/or by the presence or neurotoxic agents, such as Aβ, suggesting that diabetes and aging are risk factors for the neurodegeneration induced by these peptides [18]. Taken together, these data indicate that a correlation may exist among the age-related pathologies diabetes and AD. We have reported changes in the levels of Alzheimer's disease-related factors (such as Aβ and Tau) in vitreous bodies obtained from patients with DR, indicating that Aβ42 and Tau may be implicated in the pathogenesis of DR and that the neurodegeneration processes of DR may share, at least in part, common mechanism with Alzheimer's disease [19]. However, the detailed mechanisms are unclear at this time. Hence, the purpose of the present study was to determine the vitreous concentrations of neprilysin and Aβ in proliferative DR and to analyze the relationship between neprilysin and Aβ.

Correspondence to: Dr. Hideaki Hara, PhD, Department of Biofunctional Molecules, Gifu Pharmaceutical University, 1-5-90 Mitahora-higashi, Gifu 502-8585, Japan; Phone: +81-58-237-3931; FAX: +81-58-237-5979; email: hidehara@gifu-pu.ac.jp

METHODS

Sampling from patients: This study was conducted according to the tenets of the Declaration of Helsinki. Informed consent was obtained from all patients who underwent vitrectomy, and the study was carried out in accordance with the guidelines of the human studies committee of Kumamoto University. Patient diagnoses were idiopathic macular hole and proliferative DR (Table 1). Samples obtained from patients with a vitreous hemorrhage were not included in this study. The control group was made up of samples from eight eyes in eight patients with macular hole. Vitreous samples were also collected from ten eyes in ten patients with proliferative DR.

Measurement of neprilysin activity: Dansyl-D-Ala-Gly-p-nitro-Phe-Gly [20], Dansyl-D-Ala-Gly and thiorphan [21,22] were purchased from Sigma (st. Loius, MO). Recombinant human neprilysin was obtained from R&D Systems (Minneapolis, MN). Measurement of neprilysin activity was performed according to our previous report [23], with some modifications. In brief, 5 ml of vitreous fluid was added to 50 µl of 20 mM HEPES buffer (pH 7.2) containing a fluorescent substrate, Dansyl-D-Ala-Gly-p-nitro-Phe-Gly (200 µM), in the presence or absence of thiorphan (50 mM). Then, each sample was incubated for 60 min at 37 °C. After incubation for 5 min at 90 °C and centrifugation at 15,000 rpm for 5 min, an aliquot of the supernatant (10 µl) was used for HPLC analysis. The Dansyl-D-Ala-Gly produced from the fluorescent substrate was measured fluorometrically using an HPLC apparatus (Shimazu, RF10AXL). A reverse-phase gel column (i.e., an Inertosil-3 C18 column; 4.6 mm Φ 400 mm; GL Science) with a guard column was used for the assay. The sample was eluted using 40% (v/v) acetonitrile containing 0.05% trifluoroacetic acid at a flow rate of 0.5 ml/min at 40 °C. The amount of product was estimated by measuring its fluorescence intensity at 562 nm, with excitation at 342 nm. Protease activity (pmol/h/ml) in the vitreous fluid was estimated from the standard curve of synthetic Dansyl-D-Ala-Gly fluorescence intensity. Neprilysin-like activity (thiorphan-sensitive peptidase activity) in each sample was evaluated by subtraction of thiorphan-insensitive enzymatic activity (i.e., that recorded in the presence of thiorphan) from total activity.

Measurement of amyloid β: Specimens were collected in sterile tubes and stored at -80 °C until the analysis was conducted. Sensitive, specific enzyme-linked immunosorbent assays (ELISA) specific for Aβ42 were used for the analysis (INNOTEST β-amyloid$_{(1-42)}$; Innogenetics, Gent, Belgium). Six out of eight vitreous samples in the proliferative DR group were used to measure Aβ_{42}, because the volume of two samples was insufficient for measurement purposes. All samples were run in duplicate. The experiment was carried out in a masked fashion (by SY).

Statistical analysis: Data are expressed as means±SEM and were analyzed using a one-way ANOVA followed by a Student t-test.

Table 1. Clinical characteristics of patients

Name	Control (macular hole)	Proliferative diabetic retinopathy
n (Total)	8	10
Male	4	6
Female	4	4
Age	66.9 ± 3.1	52.2 ± 3.4

Clinical characteristics of patients with macular hole and proliferative diabetic retinopathy. Age is mean±SEM in years.

RESULTS

Neprilysin-like activity in vitreous of patients with proliferative diabetic retinopathy: The clinical characteristics of the patients providing vitreous fluid data are given in Table 1. Figure 1 shows the neprilysin-like activity levels in the vitreous of patients with macular hole (Control) or proliferative DR (Patient), with representative chromatograms for the measurement of neprilysin activity being shown in Figure 1A. The values for peptidase activity, obtained using Dansyl-D-Ala-Gly-p-nitro-Phe-Gly, in the Control group (n=8) were 0.92±0.03 and 0.77±0.04 pmol/h/µl (mean±SEM) in the absence and presence of thiorphan, respectively. In the Patient (n=10) group, the corresponding values were 1.45±0.14 and 0.75±0.03 pmol/h/µl in the absence and presence of thiorphan, respectively. There was a significant difference between the Control and Patient groups in total activity (without thiorphan), whereas the thiorphan-insensitive activities of the two groups were almost the same (Figure 1B). The values obtained for neprilysin-like peptidase activity in Control (n=8) and Patient (n=10) groups were 0.15±0.03 and 0.70±0.12 pmol/h/µl, respectively, the mean value for patients with proliferative DR being approximately 4.7 times that of the controls (Figure 1C).

Concentration of amyloid β in vitreous of patients with proliferative diabetic retinopathy: Figure 2 shows the concentrations of Aβ in the vitreous of patients with macular hole (Control) or proliferative DR (Patient). In Control (n=6) and Patient (n=10) groups, these values were 60.9±7.34 and 8.94±3.30 pg/ml, respectively, the latter value being significantly smaller than the former.

Relationship between neprilysin-like activity and amyloid β concentration in vitreous: Figure 3 shows that neprilysin-like peptidase activity was elevated and, in contrast, the Aβ concentration was reduced in the vitreous of proliferative DR patients (versus the controls). There was a significant inverse correlation ($y=-0.0089x + 0.7472$, $p=0.0072$, $R^2=0.4134$) between neprilysin-like peptidase activity and Aβ concentration among all subjects.

DISCUSSION

In this study, we observed a significant increase in neprilysin-like peptidase activity and a significant reduction in Aβ concentration in the vitreous fluid of patients with proliferative DR (by comparison with macular hole patients), and a significant inverse correlation was revealed between these two parameters in vitreous fluid.

Recent reports [19,24-27] suggest that Aβ increases in various areas of the eye during the progression of eye diseases, and therefore that the increase in Aβ might contribute to the eye disease. Interestingly, Aβ deposition has been reported to be specific to drusen in the eyes of patients with age-related macular degeneration (AMD) [24-26], suggesting that Aβ might be associated with the more advanced stages of AMD [26]. AMD is a retinal degenerative disease that leads to a loss of central vision, and it affects 5-10% of the population over 60 years of age. A number of studies have confirmed that the presence of drusen-identified as gray-yellow deposits that collect in or around the macula of the retina-represents a significant risk factor for the development of visual loss from AMD [28-30]. Goldstein et al. [27] noted that Aβ is present in the cytosol of lens fiber cells in patients with AD and that the presence of Aβ in the lens might promote regionally specific lens protein aggregation, extracerebral amyloid formation and supranuclear cataracts. Recently, an association between diabetes mellitus and an increased risk of developing AD has been suggested (i.e., diabetes mellitus may be associated with the development of AD and with the decline in cognitive function in older persons) [31]. We reported recently that the concentrations of Aβ42 and tau showed a decrease and an increase, respectively (versus macular hole controls), in the vitreous fluid from patients with glaucoma and DR [19]. However, there have been no previous reports regarding changes in neprilysin in eye diseases.

An increase in TUNEL-positive cells in retinal neurons has been observed at an early stage in streptozotocin-diabetic rats and in human diabetes, and neurodegeneration may be an important component of DR [32]. Given our finding that a decrease in the concentration of Aβ42 in the vitreous fluid obtained from patients with DR is observed regardless of the manner of the disease progression (proliferative or edematous), it is possible that factors associated with the early stages of diabetes development may affect Aβ metabolism in the retina,

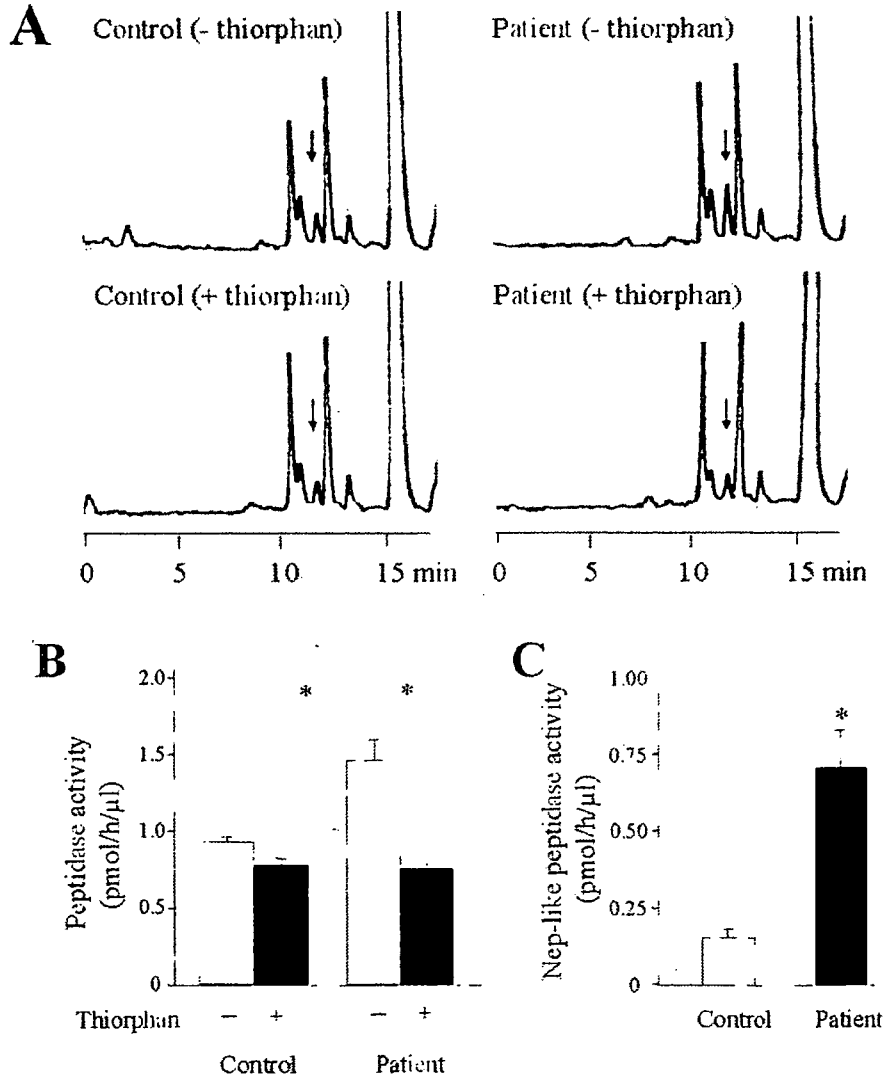

Figure 1. Neprilysin-like peptidase activity in vitreous samples. Neprilysin-like peptidase activity was measured in vitreous samples obtained from patients with macular hole (Control) or proliferative diabetic retinopathy (Patient). **A**: Representative chromatograms for measurement of neprilysin activity. Arrows indicate the product, Dansyl-D-Ala-Gly. **B**: Peptidase activity in the absence (open column) or presence (solid column) of thiorphan was measured by means of an HPLC-fluorometric system, as described under Materials and Methods. **C**: Neprilysin-like peptidase activity was calculated by subtraction of thiorphan-insensitive peptidase activity from total activity. Values are mean±SEM, n=8 (Control) and 10 (Patient). Asterisk (*) represents $p<0.001$ (Student t-test).

possibly leading to neurodegeneration in DR. Further studies will be needed for a full elucidation of the alterations in Aβ in DR.

Recently, we established a novel, sensitive protocol for the measurement of extracellular cell-surface neprilysin activity in living cells (using an HPLC apparatus) [23]. Using this system, we investigated the effect of hypoxia on neprilysin activity in human neuroblastoma SH-SY5Y cells, and we demonstrated that hypoxia (under 5% O_2 for 24 h)-an event closely associated with DR and neurodegenerative diseases-significantly attenuated neprilysin activity without any alteration in neprilysin gene expression [23]. Neprilysin is reported to be secreted from LLC-PK1 cells (originate from pig proximal tubule of the nephron) [33], human prostatic secretory cells [34] and invasive human melanoma cell lines [35]. In case of prostatic tissue, neprilysin is released from the cells in an apocrine fashion [34]. Recently, it was shown that cerebrospinal fluid (CSF) neprilysin elevates with the progression of Alzheimer's disease, and suggested that presynaptically located neprilysin could be released into CSF as a consequence of synaptic disruption [36]. Therefore, one possibility is that under a hypoxic condition, neprilysin is released from membrane, with the result that soluble neprilysin is increased at the extracellular level.

A limitation of the present study is the small sample sizes. Nevertheless, we observed an apparent relationship between increased neprilysin-like peptidase activity and decreased Aβ concentration in patients with proliferative DR. On the basis of the present data, we can speculate about the underlying mechanism as follows. One of many possible reasons for this observation is degradation of Aβ by neprilysin. Namely, retinal damage is induced by DR, and consequently the neprilysin bound to the membrane of the retinal cells is cleaved off, thereby increasing the concentration of soluble neprilysin within the vitreous body. If membrane-anchored neprilysin serves to offer a locus for the degradation of newly generated Aβ within the synapse, any neprilysin separated from the cell membrane will not be able to perform its role of scavenging synaptic Aβ molecules. It is possible that a decrease in cell-surface neprilysin causes an enhancement of Aβ aggregation within the synapse and a degeneration of ganglion cells within the retina. This hypothesis is consistent with the observation of a decrease in Aβ42 in the vitreous of patients with proliferative DR since some might form aggregates on the membrane of retinal cells, while others might be degraded by soluble neprilysin within the vitreous.

There are other possible mechanisms, as follows: in DR patients, Aβ accumulates the retina for some reason and consequently Aβ and neprilysin levels in the vitreous decrease and increase, respectively. Aβ is reportedly detected in retinal ganglion cells (by immunohistochemistry) significantly more often in ocular hypertensive retinas than in control retinas [37]. Further work will be necessary to determine whether the decrease in the Aβ level really is related to the increase in neprilysin activity.

In conclusion, neprilysin activity and Aβ concentrations displayed converse changes in patients with proliferative DR, there being a significant inverse correlation between the two parameters.

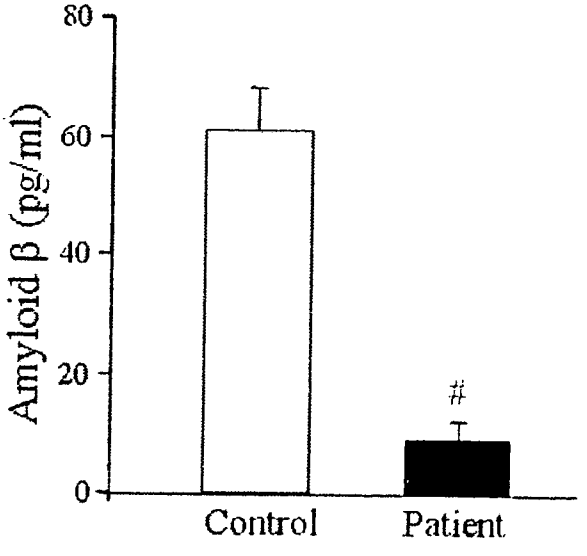

Figure 2. Concentrations of β-amyloid$_{(1-42)}$ (Aβ42) in vitreous samples. Aβ42 was measured in vitreous samples obtained from patients with macular hole (Control) or proliferative diabetic retinopathy (Patient) by use of sensitive, specific enzyme-linked immunosorbent assays (ELISA), as described under Methods. Values are mean±SEM, n=6 (Control) and 10 (Patient). Sharp (#) indicates p<0.0001 for comparison to control (Student t-test).

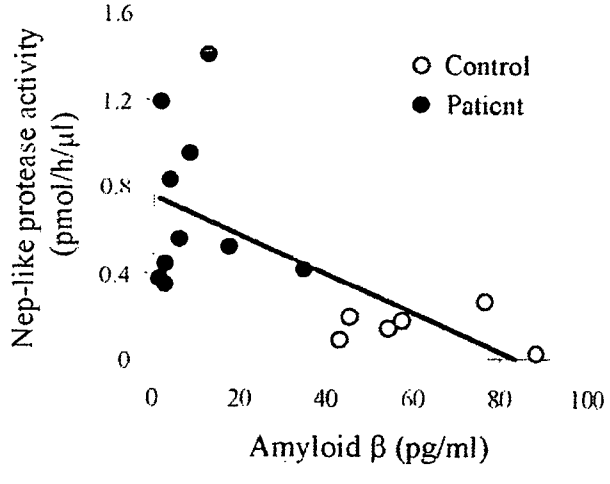

Figure 3. Relationship between neprilysin-like peptidase activity and amyloid β concentration in vitreous. Neprilysin-like peptidase activity was elevated and, in contrast, Aβ was reduced in the vitreous of proliferative DR patients (versus Control). There was a significant inverse correlation (y=-0.0089x + 0.7472, p=0.0072, R^2=0.4134) between neprilysin-like peptidase activity and Aβ among all subjects.

ACKNOWLEDGEMENTS

This study was supported by the Gifu Prefecture Research Foundation and the Naito Foundation.

REFERENCES

1. Engerman RL, Kern TS. Experimental galactosemia produces diabetic-like retinopathy. Diabetes 1984; 33:97-100.
2. Mizutani M, Kern TS, Lorenzi M. Accelerated death of retinal microvascular cells in human and experimental diabetic retinopathy. J Clin Invest 1996; 97:2883-90.
3. Kern TS, Tang J, Mizutani M, Kowluru RA, Nagaraj RH, Romeo G, Podesta F, Lorenzi M. Response of capillary cell death to aminoguanidine predicts the development of retinopathy: comparison of diabetes and galactosemia. Invest Ophthalmol Vis Sci 2000; 41:3972-8.
4. De Strooper B, Annaert W. Proteolytic processing and cell biological functions of the amyloid precursor protein. J Cell Sci 2000; 113:1857-70.
5. Selkoe DJ. Alzheimer's disease: genes, proteins, and therapy. Physiol Rev 2001; 81:741-66.
6. Iwata N, Tsubuki S, Takaki Y, Watanabe K, Sekiguchi M, Hosoki E, Kawashima-Morishima M, Lee HJ, Hama E, Sekine-Aizawa Y, Saido TC. Identification of the major Abeta1-42-degrading catabolic pathway in brain parenchyma: suppression leads to biochemical and pathological deposition. Nat Med 2000; 6:143-50.
7. Turner AJ, Isaac RE, Coates D. The neprilysin (NEP) family of zinc metalloendopeptidases: genomics and function. Bioessays 2001; 23:261-9.
8. Iwata N, Tsubuki S, Takaki Y, Shirotani K, Lu B, Gerard NP, Gerard C, Hama E, Lee HJ, Saido TC. Metabolic regulation of brain Abeta by neprilysin. Science 2001; 292:1550-2.
9. Iwata N, Mizukami H, Shirotani K, Takaki Y, Muramatsu S, Lu B, Gerard NP, Gerard C, Ozawa K, Saido TC. Presynaptic localization of neprilysin contributes to efficient clearance of amyloid-beta peptide in mouse brain. J Neurosci 2004; 24:991-8.
10. Yasojima K, Akiyama H, McGeer EG, McGeer PL. Reduced neprilysin in high plaque areas of Alzheimer brain: a possible relationship to deficient degradation of beta-amyloid peptide. Neurosci Lett 2001; 297:97-100.
11. Van Broeckhoven C, Genthe AM, Vandenberghe A, Horsthemke B, Backhovens H, Raeymaekers P, Van Hul W, Wehnert A, Gheuens J, Cras P, Bruyland M, Martin JJ, Salbaum M, Multhaup G, Masters CL, Beyreuther K, Gurling HMD, Mullan MJ, Holland A, Barton A, Irving N, Williamson R, Richards SJ, Hardy JA. Failure of familial Alzheimer's disease to segregate with the A4-amyloid gene in several European families. Nature 1987; 329:153-5.
12. Tanzi RE, St George-Hyslop PH, Haines JL, Polinsky RJ, Nee L, Foncin JF, Neve RL, McClatchey AI, Conneally PM, Gusella JF. The genetic defect in familial Alzheimer's disease is not tightly linked to the amyloid beta-protein gene. Nature 1987; 329:156-7.
13. St George-Hyslop PH, Haines JL, Farrer LA, Polinsky R, Van Broeckhoven C, Goate A, McLachlan DR, Orr H, Bruni AC, Sorbi S, Rainero I, Foncin JF, Pollen D, Cantu JM, Tupler R, Voskresenskaya N, Mayeux R, Growdon J, Fried VA, Myers RH, Nee L, Backhovens H, Martin JJ, Rossor M, Owen MJ, Mullan M, Percy ME, Karlinsky H, Rich S, Heston L, Montesi M, Mortilla M, Nacmias N, Gusella JF, Hardy JA. Genetic linkage studies suggest that Alzheimer's disease is not a single homogeneous disorder. FAD Collaborative Study Group. Nature 1990; 347:194-7.
14. Wilson PW, Anderson KM, Kannel WB. Epidemiology of diabetes mellitus in the elderly. The Framingham Study. Am J Med 1986; 80:3-9.
15. Barnett AH, Eff C, Leslie RD, Pyke DA. Diabetes in identical twins. A study of 200 pairs. Diabetologia 1981; 20:87-93.
16. Newman B, Selby JV, King MC, Slemenda C, Fabsitz R, Friedman GD. Concordance for type 2 (non-insulin-dependent) diabetes mellitus in male twins. Diabetologia 1987; 30:763-8.
17. Janson J, Laedtke T, Parisi JE, O'Brien P, Petersen RC, Butler PC. Increased risk of type 2 diabetes in Alzheimer disease. Diabetes 2004; 53:474-81.
18. Moreira PI, Santos MS, Moreno AM, Seica R, Oliveira CR. Increased vulnerability of brain mitochondria in diabetic (Goto-Kakizaki) rats with aging and amyloid-beta exposure. Diabetes 2003; 52:1449-56.
19. Yoneda S, Hara H, Hirata A, Fukushima M, Inomata Y, Tanihara H. Vitreous fluid levels of beta-amyloid((1-42)) and tau in patients with retinal diseases. Jpn J Ophthalmol 2005; 49:106-8.
20. Florentin D, Sassi A, Roques BP. A highly sensitive fluorometric assay for "enkephalinase," a neutral metalloendopeptidase that releases tyrosine-glycine-glycine from enkephalins. Anal Biochem 1984; 141:62-9.
21. Dolev I, Michaelson DM. A nontransgenic mouse model shows inducible amyloid-beta (Abeta) peptide deposition and elucidates the role of apolipoprotein E in the amyloid cascade. Proc Natl Acad Sci U S A 2004; 101:13909-14.
22. Roques BP, Fournie-Zaluski MC, Soroca E, Lecomte JM, Malfroy B, Llorens C, Schwartz JC. The enkephalinase inhibitor thiorphan shows antinociceptive activity in mice. Nature 1980; 288:286-8.
23. Oh-hashi K, Nagai T, Tanaka T, Yu H, Hirata Y, Kiuchi K. Determination of hypoxic effect on neprilysin activity in human neuroblastoma SH-SY5Y cells using a novel HPLC method. Biochem Biophys Res Commun 2005; 334:380-5.
24. Johnson LV, Leitner WP, Rivest AJ, Staples MK, Radeke MJ, Anderson DH. The Alzheimer's A beta-peptide is deposited at sites of complement activation in pathologic deposits associated with aging and age-related macular degeneration. Proc Natl Acad Sci U S A 2002; 99:11830-5.
25. Dentchev T, Milam AH, Lee VM, Trojanowski JQ, Dunaief JL. Amyloid-beta is found in drusen from some age-related macular degeneration retinas, but not in drusen from normal retinas. Mol Vis 2003; 9:184-90.
26. Anderson DH, Talaga KC, Rivest AJ, Barron E, Hageman GS, Johnson LV. Characterization of beta amyloid assemblies in drusen: the deposits associated with aging and age-related macular degeneration. Exp Eye Res 2004; 78:243-56.
27. Goldstein LE, Muffat JA, Cherny RA, Moir RD, Ericsson MH, Huang X, Mavros C, Coccia JA, Faget KY, Fitch KA, Masters CL, Tanzi RE, Chylack LT Jr, Bush AI. Cytosolic beta-amyloid deposition and supranuclear cataracts in lenses from people with Alzheimer's disease. Lancet 2003; 361:1258-65.
28. Bird AC, Bressler NM, Bressler SB, Chisholm IH, Coscas G, Davis MD, de Jong PT, Klaver CC, Klein BEK, Klein R, Mitchell P, Sarks JP, Sarks SH, Soubrane G, Taylor HR, Vingerling JR. An international classification and grading system for age-related maculopathy and age-related macular degeneration. The International ARM Epidemiological Study Group. Surv Ophthalmol 1995; 39:367-74.
29. Smiddy WE, Fine SL. Prognosis of patients with bilateral macular drusen. Ophthalmology 1984; 91:271-7.

30. Wang JJ, Foran S, Smith W, Mitchell P. Risk of age-related macular degeneration in eyes with macular drusen or hyperpigmentation: the Blue Mountains Eye Study cohort. Arch Ophthalmol 2003; 121:658-63.
31. Arvanitakis Z, Wilson RS, Bienias JL, Evans DA, Bennett DA. Diabetes mellitus and risk of Alzheimer disease and decline in cognitive function. Arch Neurol 2004; 61:661-6.
32. Barber AJ, Lieth E, Khin SA, Antonetti DA, Buchanan AG, Gardner TW. Neural apoptosis in the retina during experimental and human diabetes. Early onset and effect of insulin. J Clin Invest 1998; 102:783-91.
33. Lanctot C, Fournier H, Howell S, Boileau G, Crine P. Direct targeting of neutral endopeptidase (EC 3.4.24.11) to the apical cell surface of transfected LLC-PK1 cells and unpolarized secretion of its soluble form. Biochem J 1995; 305:165-71.
34. Renneberg H, Albrecht M, Kurek R, Krause E, Lottspeich F, Aumuller G, Wilhelm B. Identification and characterization of neutral endopeptidase (EC 3. 4. 24. 11) from human prostasomes—localization in prostatic tissue and cell lines. Prostate 2001; 46:173-83.
35. Saghatelian A, Jessani N, Joseph A, Humphrey M, Cravatt BF. Activity-based probes for the proteomic profiling of metalloproteases. Proc Natl Acad Sci U S A 2004; 101:10000-5.
36. Maruyama M, Higuchi M, Takaki Y, Matsuba Y, Tanji H, Nemoto M, Tomita N, Matsui T, Iwata N, Mizukami H, Muramatsu S, Ozawa K, Saido TC, Arai H, Sasaki H. Cerebrospinal fluid neprilysin is reduced in prodromal Alzheimer's disease. Ann Neurol 2005; 57:832-42.
37. McKinnon SJ, Lehman DM, Kerrigan-Baumrind LA, Merges CA, Pease ME, Kerrigan DF, Ransom NL, Tahzib NG, Reitsamer HA, Levkovitch-Verbin H, Quigley HA, Zack DJ. Caspase activation and amyloid precursor protein cleavage in rat ocular hypertension. Invest Ophthalmol Vis Sci 2002; 43:1077-87.

The print version of this article was created on 17 Aug 2006. This reflects all typographical corrections and errata to the article through that date. Details of any changes may be found in the online version of the article.

Available online at www.sciencedirect.com
ScienceDirect
Experimental Eye Research 83 (2006) 1396–1404
EXPERIMENTAL EYE RESEARCH
www.elsevier.com/locate/yexer

Induction of matrix metalloproteinases (MMPs) and tissue inhibitors of MMPs correlates with outcome of acute experimental pseudomonal keratitis

Kousuke Ikema [a], Koki Matsumoto [a,*], Yasuya Inomata [a], Yoshihiro Komohara [b], Seiya Miyajima [a], Motohiro Takeya [b], Hidenobu Tanihara [a]

[a] *Department of Ophthalmology and Visual Science, Kumamoto University Graduate School of Medical Sciences, 1-1-1, Honjo, Kumamoto 860-0811, Japan*
[b] *Department of Cell Pathology, Kumamoto University Graduate School of Medical Sciences, 1-1-1, Honjo, Kumamoto 860-0811, Japan*

Received 25 January 2006; accepted in revised form 19 July 2006
Available online 11 September 2006

Abstract

This study aimed to investigate expressions and sources of matrix metalloproteinases (MMP)-2 and MMP-9, and of tissue inhibitors of MMP (TIMP)-1 and TIMP-2 in experimental *Pseudomonas aeruginosa* keratitis in rabbits. Pseudomonal keratitis was induced in New Zealand white rabbits, and macroscopic and microscopic examinations were performed at appropriate time points (3, 9, 12, 18, 24, 72 h). Expressions and sources of MMP-2, 9, and TIMP-1, 2 were determined using immunohistochemistry, gelatin zymography, ELISA, and RT-PCR. A typical corneal ulcer with a ring abscess was observed 12–72 h post-infection (p.i.) with *P. aeruginosa*. In microscopic examinations, massive inflammatory cell (mostly polymorphonuclear leukocytes, PMNs) infiltration and liquefactive necrosis were characteristic features. MMP-2 was constitutively expressed in keratocytes, and its expression was not apparently enhanced after pseudomonal infection as evidenced by zymography, immunostaining, and RT-PCR. However, MMP-9 and its activated form were induced, and were significantly enhanced 12–24 h p.i. MMP-9 appeared to derive from PMNs rather than from resident corneal cells. TIMP-1 was expressed in PMNs, macrophages, and keratocytes, and its expression was enhanced 72 h p.i. Although TIMP-2 was constitutively expressed as seen by immunostaining and RT-PCR, its concentration was below detection limits during the experiments. We demonstrated that MMP-9 was one of the important factors for corneal tissue destruction, because it was induced and significantly expressed in keratocytes and inflammatory cells after pseudomonal infection. Although TIMP-1 was expressed in later stages of infection, enhancement and activation of MMP-9 were much faster and stronger than those of TIMP-1, thereby facilitating tissue destruction leading to corneal ulceration.

Keywords: pseudomonal keratitis; MMP-2; MMP-9; TIMP-1; TIMP-2

1. Introduction

Keratitis caused by *Pseudomonas aeruginosa* is rapidly progressive, resistant to even vigorous treatments, and often results in corneal perforation and loss of vision (Laibson, 1972). Recently, increasing cases of pseudomonal keratitis have been observed in contact lens wearers, especially those with extended wear of soft contact lenses (Alfonso et al., 1986). Furthermore, overnight orthokeratology lens wear is another risk factor for pseudomonal keratitis (Ladage et al., 2004; Lau et al., 2003; Tabbara et al., 2000; Wang and Lim, 2003; Young et al., 2003).

Pseudomonal keratitis is characterized by corneal ulcers with a ring abscess in contrast to keratitis due to gram-positive cocci exhibiting localized abscesses (Matsumoto, 2000).

* Corresponding author. Tel.: +81 96 373 5247; fax: +81 96 373 5249.
E-mail address: matsumoto@ntthosp.jp (K. Matsumoto).

0014-4835/$ - see front matter © 2006 Elsevier Ltd. All rights reserved.
doi:10.1016/j.exer.2006.07.019

We previously reported that tissue destruction seen in *P. aeruginosa* corneal infections might result from enhanced expression of matrix metalloproteinases (MMPs) by keratocytes stimulated by exoproteases and proinflammatory cytokines, and proteolytic activation of MMPs by pseudomonal elastase (Matsumoto et al., 1992). We further reported that pseudomonal virulence factors (pseudomonal elastase, alkaline protease, and lipopolysaccharides), and inflammatory cytokines (interleukin-1β and tumor necrosis factor-α) enhanced expression of both MMP-2 and MMP-9 in cultured rabbit corneal fibroblasts (Miyajima et al., 2001). MMPs are a family of enzymes capable of degrading extracellular matrices. Most of MMPs are secreted as latent precursors, and need to be activated before performing their functions. MMP-2 and MMP-9 are independent gene products, and have unique substrate specificities. On the contrary, tissue inhibitors of MMPs (TIMPs) are major endogenous regulators of MMP activity in tissues (Opbroek et al., 1993). To date, 4 distinctive TIMPs (TIMP-1, -2, -3, and -4) have been identified. TIMP-1 binds to the inactive precursor of MMP-9, and to active forms of other MMPs (Wilhelm et al., 1989). TIMP-1 is believed to bind to the active site of MMP-2 following molecular stabilization due to binding of TIMP-2 to MMP-2 (Woessner, 1991). TIMP-2 is known to bind to MMP-2 with a 1:1 molar ratio (Goldberg et al., 1989).

This study aimed to investigate expressions and sources of MMPs (MMP-2 and MMP-9) and TIMPs (TIMP-1 and TIMP-2) in experimental pseudomonal keratitis in rabbits, to elucidate roles of these proteins in corneal ulceration.

2. Materials and methods

2.1. Animals

Female New Zealand albino rabbits ($n = 45$) weighing 1.7–2.2 kg were used in this study. Animals were housed under a well-conditioned atmosphere in the Center of Animal Resources and Development at Kumamoto University. Animals were handled and treated humanely, and experiments adhered to the Guidelines of ARVO for the use of animals. Experimental protocols were approved by the ethics committees of the University.

2.2. Preparation of bacteria and pseudomonal keratitis in rabbits

Pseudomonas aeruginosa Ueno strain, which was isolated from a patient with bilateral corneal ulcers, produces both elastase and alkaline protease. This strain was cultured in trypticase soy broth (Sigma St. Louis, Mo) for 12 h at 35 °C, with reciprocal shaking at 60 Hz. Bacteria were washed 3 times with sterile physiological saline, and concentration of the bacterial suspension was adjusted to 2×10^6 CFU/ml using a standard curve correlating viable cell numbers to optical density at 600 nm. Once rabbits were systemically anesthetized with ketamine hydrochloride and sodium pentobarbital, and topically with oxybuprocaine hydrochloride, samples of *P. aeruginosa* at 2×10^4 CFU/μl were injected into the corneal stroma in right eyes, using a 30-G needle connected to a microsyringe. Sterile physiological saline was similarly injected into the left eyes of 3 rabbits as controls.

2.3. Macroscopic observations of keratitis

Corneal lesions were macroscopically observed at appropriate times (3, 9, 12, 18, 24, and 72 h after bacterial infection), and were photographed. Observations were done in triplicates at each time point.

2.4. Histopathology and Immunohistochemistry

For histopathological examinations, enucleated eyes at appropriate times ($n = 6$ for 3, 9, 12, 18, 24, and 72 h p.i.) were fixed in 8% paraformaldehyde, and embedded in paraffin. Five-μm tissue sections were cut using a microtome, and were mounted on APS-coated micro-glass slides. Specimens were stained with hematoxylin and eosin.

For immunohistochemistry, enucleated eyes ($n = 5$ for 3, 12, 24, and 72 h p.i. and the control sample) were fixed with periodate-lysine-paraformaldehyde (PLP) fixative, and were embedded in optimal cutting temperature (O.C.T) compound. Samples were immediately frozen in liquid nitrogen, and stored at −80 °C. Six-μm frozen sections were cut from each block, and were immunostained with anti-human MMP-2, -9, TIMP-1 and -2 mouse monoclonal antibodies (DAIICHI Fine Chemical Co., Ltd, Toyama, Japan). They were visualized using diaminobenzidine (DAB) detection methods. All antibodies were diluted in PBS to the proper concentrations. Goat anti-mouse IgG antibody (Nichirei, Tokyo, Japan) was used as secondary antibody. As negative control, non-specific mouse IgG1 (Dako Cytomation, Kyoto, Japan) was used as primary antibody. Furthermore, to clarify whether macrophages expressed MMP-9, double immunostaining was performed using a specific antibody against the macrophage surface marker, RbM2. Once sections were immunostained and visualized using the DAB detection system, as described above, they were soaked in glycine for 30 min to remove non-specific binding of the secondary antibody. Then, they were washed with PBS, and were blocked with 5% goat serum. Sections were immunostained with RbM2, (mouse monoclonal antibody, Trans Genic Inc., Hyogo, Japan) and were visualized using alkaline phosphatase (AP) with BCIP/NBT (5-Bromo-4-Chloro-3-Indoxyl Phosphate/Nitro Blue Tetrazolium Chloride, DakoCytomation, Kyoto, Japan). A goat anti-mouse IgG antibody (Nichirei, Tokyo, Japan) was used as secondary antibody. Three negative controls without primary antibodies for MMP-9, RbM2, and both were also included.

2.5. Gelatin zymography

Zymography was performed using the method of Heussen and Dowdle (1980) with some modifications. Gelatin was

used as substrate at a final concentration of 0.1%. As described previously (Matsumoto et al., 1993), excised corneas were treated with 2% SDS for 1 h at room temperature, and were centrifuged at 15 000 rpm for 10 min. Supernatants were mixed with sample buffer, and were applied to a SDS PAGE gel containing the substrates. Electrophoresis was performed at 4 °C. All lanes were loaded with the same amounts of proteins. Following electrophoresis, gels were rinsed with 2.5% Triton X-100 (with or without 100 mM EDTA) for 1 h at room temperature to remove SDS. Gels were incubated in reaction buffer (50 mM Tris–HCl, pH 6.8 containing 10 mM $CaCl_2$) with or without 100 mM EDTA overnight at 37 °C. Once the gels were stained with Coomassie brilliant blue R250, proteins possessing gelatinolytic activity could be easily identified as clear lytic bands against background. Prestained standard proteins were used as molecular weight markers.

2.6. Quantification of TIMP-1 and TIMP-2

Corneal extracts obtained by homogenization and centrifugation ($n = 4$ at each time point) were added to TIMP-1 immunoassay plates (TIMP-1 ELISA kit, DAIICHI Fine Chemical Co., Ltd, Toyama, Japan) and TIMP-2 coated beads (TIMP-2 ELISA kit, DAIICHI Fine Chemical Co., Ltd, Toyama, Japan). Analysis was performed according to the manufacturer's protocols. Obtained values were revised with each corresponding sample's protein concentration. Detection limits of the systems for TIMP-1 and -2 were 51–2000 ng/ml and 20–320 ng/ml, respectively. The Fisher's method was used for statistical analysis.

2.7. Expressions and quantifications of MMP-2, -9; and TIMP-1, and -2 mRNAs

Expressions and quantifications of mRNAs for MMP-2, -9; and TIMP-1, -2 were analyzed using RT-PCR. Portions of excised corneas ($n = 4$ for each time point and control; 3, 12, 24, and 72 h p.i.) were soaked in RNA STAT-60® (TEL-TEST, INC. Los Angeles, CA), and were manually homogenized. Total RNAs were isolated according to the following procedures: chloroform was added to RNA STAT-60®, and the mixture was shaken. Homogenates were then centrifuged at 15 000 rpm for 15 min at 4 °C. The aqueous phase was transferred into a clean tube, and was mixed with isopropanol. Samples were then centrifuged at 15 000 rpm (for 10 min), and supernatants were removed. Pelleted RNA samples were washed with ethanol. RNA samples were dissolved in diethylpyrocarbonate (DEPC)-treated water. Using RNA templates obtained in this way, reverse transcription was performed to obtain complementary DNAs (cDNAs) according to the manufacturer's protocols (QIAGEN Omni script RT kit. Tokyo, Japan). RT-PCR was then performed. Primer sequences and PCR conditions for each gene studied are described in Table 1 (Berceli et al., 2004). Ten-μl samples of each PCR product were applied to a 3-% agarose gel, electrophoresed, stained with ethidium bromide, and photographed.

Furthermore, using the cDNA templates, real time PCR (Taqman PCR analysis) was performed according to the manufacturer's protocols (TaKaRa bio. Premix Ex Taq™ Tokyo, Japan). Assays were performed using the ABI PRISM® 7000 Sequence Detection System (Applied Biosystems). For MMP-2, 5′-CAAGTGGGACAAGAATCAGATCACA was used as forward primer, 5′-GAAGGCATCATCCACTGT TTCC as reverse primer and 5′-ACACGCCTGACCTCGAC as probe. For MMP-9, 5′-CCGCCAGCCCACCTT was used as forward primer, 5′-GTCGGTGAGCCTGGTTCTC as reverse primer and 5′-TCTCCTGGGAAGACCAC as probe. For TIMP-1, 5′-CTGGAACAGTCTGAGCTTCTCT was used as forward primer, 5′-CCGGCAGCGTAGGTCTT as reverse primer and 5′-AACGTTCCGGCTTCACC as probe. For TIMP-2, 5′-CCCATCAAGAGGATCCAGTATGAGA was used as forward primer, 5′-GTGTAGATGAACTCGA TGTCCTTGT as reverse primer and 5′-CAAGCAGATCAA GATGTTC as probe (Custom Taqman Gene Expression Assay Service, Applied Biosystems. Foster City, CA). The probes were labeled with a FAM dye. All quantitative PCR assays were performed in duplicates. Results were expressed as ratios of target gene mRNA copies to 18S ribosomal RNA (Applied Biosystems, Foster City, CA) copies.

3. Results

3.1. Macroscopic examinations

By 3 h after bacterial infection, no significant changes except for mild conjunctival infection compared to saline-injected control corneas (Fig. 1A) were observed (Fig. 1B). At 9 h p.i., mild corneal opacity was seen at the injection site (Fig. 1C). However, no corneal epithelial defect nor inflammatory cells in the anterior chamber was detected. Twelve to 18 h p.i., corneal ulcers with typical ring abscesses and severe chemosis were observed (Fig. 1D). Detailed observation of the anterior chamber could not be performed due to severe corneal opacity. At 24 h p.i., most of corneal ulcers extended further to perforation (Fig. 1E). The peripheral cornea showed a ground glass appearance. Anterior chamber information could not be obtained. At 72 h p.i., corneal lesions further deteriorated, and the entire cornea became opaque (Fig. 1F).

3.2. Histopathology

By 3 h p.i., no remarkable changes were observed. Apparent inflammatory cell infiltration was observed in the anterior stroma near the limbus 9–12 h p.i. (Fig. 2A). At 12 h p.i., some inflammatory cells accumulated around the injection site. At 24 h p.i., marked corneal stromal swelling with massive inflammatory cell infiltration was observed in the center of the cornea (Fig. 2B). Furthermore, liquefactive necrosis was seen inside a massive inflammatory cell infiltrated site (Fig. 2B). At higher magnification, most of inflammatory cells were identified as polymorphonuclear leukocytes (PMNs), and numerous bacteria could be seen (Fig. 2B, inset). These

Table 1
Primer sequences and amplification conditions for RT-PCR

Gene	Primer sequence	Annealing temp. (°C)	Optimal cycle	Base pair
MMP-2	AGAAGATCGACGCTGTACGAGGCTGAATACACCCAGTATTCATTG	60	35	83
MMP-9	CCGGCATTCAGGGAGATGTCGGCGTTTCCAAAGTACG	60	31	91
TIMP-1	CGCAGCGAGGAGTTTCTCACAAGTCGTGATGTGCAAGAG	55	28	62
TIMP-2	GAGATCAAGCAGATCAAGATGTTCAGGACGGCGCTGTGTAGATG	55	33	69

corneal lesions further progressed to prominent liquefactive necrosis 24–72 h p.i. (data not shown).

3.3. Immunohistochemistry

MMP-2 labeling was very faint in keratocytes in the central cornea, and around the limbus at 3 h and 12 h p.i. (data not shown). At 24 h and 72 h p.i., no remarkable labeling for MMP-2 was observed even in the central cornea where liquefactive necrosis had formed. However, significant MMP-2 staining was observed in keratocytes close to the limbus (Fig. 3A). On the other hand, MMP-9 was mainly observed in PMNs from the early phases of infection, and labeling intensity gradually increased with time. MMP-9 labeling was also observed in macrophages and keratocytes. Using double immunostaining methods, MMP-9 was detected around macrophages (Figs. 3B and C). Although MMP-9 immunostaining showed high intensity near the limbus (Fig. 3B), its intensity decreased in the central cornea, where marked liquefactive necrosis was seen 24–72 h p.i. (data not shown).

TIMP-1 was present in keratocytes and macrophages near the corneal limbus at 12–72 h p.i. (Fig. 3D). However, staining was very faint in the central cornea during the infection course (data not shown). TIMP-2 was detected in PMNs close to the limbus 12–24 h p.i. (Fig. 3E), but labeling decreased thereafter. On the contrary, around the central cornea, TIMP-2 labeling gradually increased as PMNs accumulated at the injection site 12–72 h p.i. (data not shown). All negative controls showed no detectable levels of labeling (data not shown).

3.4. Gelatin zymography

Precursor of MMP-2 (proMMP-2) was detected even in control samples (Fig. 4). In infected corneal extracts, proMMP-2 was detected 3–24 h p.i., and its activity was slightly increased at 72 h p.i. (Fig. 4). The active form was faintly detected from 12 h p.i. On the other hand, proMMP-9 and its active form were detected at 12 h p.i., and their activities significantly increased thereafter (Fig. 4). On the contrary, gels which were washed and reacted in the presence of 100 mM EDTA showed no clear lytic bands (data not shown).

3.5. Quantification of TIMP-1 and TIMP-2

TIMP-1 and TIMP-2 were quantified using an ELISA detection system kit. Concentrations of TIMP-1 at 3 and 12 h p.i. were below detection limits. Those at 24 and 72 h p.i. were 55.0 ± 8 ng/ml and 161.5 ± 33.7 ng/ml, respectively (Fig. 5). There were statistically significant differences in concentration between these 2 time points (Fisher's test, $p < 0.0001$). On the contrary, concentration of TIMP-2 was below detection limits at any time points using the ELISA kit (Fig. 5).

3.6. Expression of MMP and TIMP mRNAs

MMP-2 mRNA was detected in control and infected samples obtained at 3, 12, 24, and 72 h p.i., and its relative concentration was almost constant (Fig. 6). MMP-9 mRNA was faintly detected in control and infected samples obtained (Fig. 6) at 3 h p.i. However, its expression was clearly

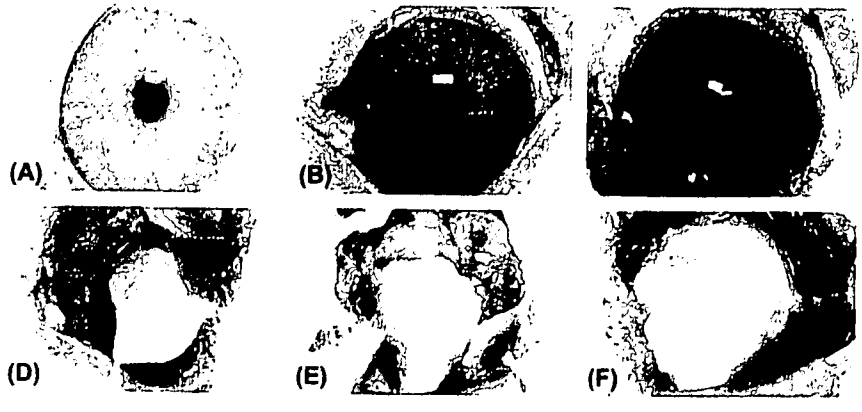

Fig. 1. Macroscopic observations of keratitis caused by *Pseudomonas aeruginosa* in rabbits. (A) Control cornea injected with saline. (B) Corneal lesion 3 h post injection (p.i.); (C) 9 h p.i.; (D) 12 h p.i.; (E) 24 h p.i.; and (F) 72 h p.i. Note that the corneal ulcer with a typical ring abscess is observed at 24–72 h p.i.

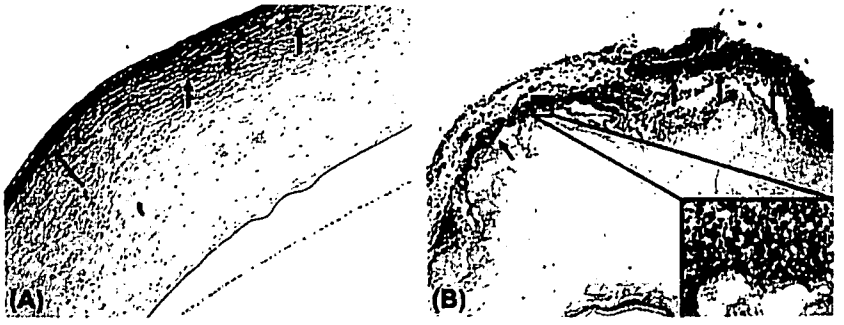

Fig. 2. Microscopic observations of keratitis caused by *P. aeruginosa*. (A) 9 h p.i. in the peripheral cornea. (×100). (B) 24 h p.i. in the central cornea (inset), higher magnification of Fig. 2B (×1000). Note the massive inflammatory cell infiltration and liquefactive necrosis. Most inflammatory cells were identified as PMNs (black arrows).

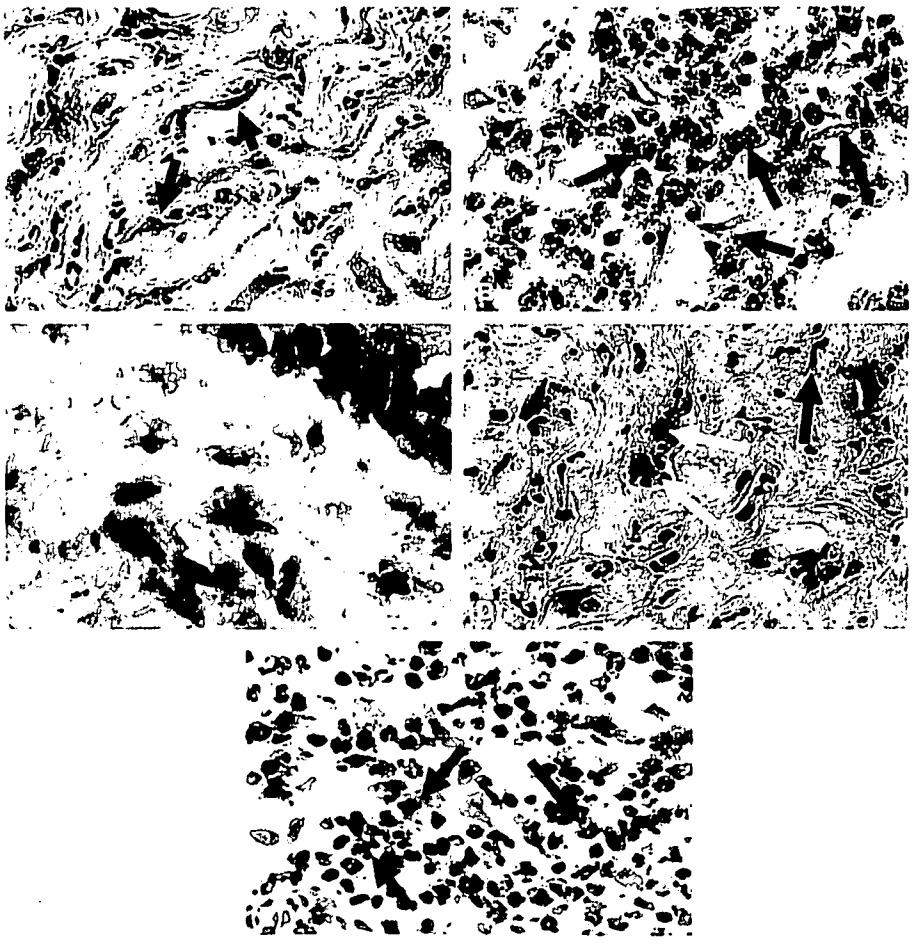

Fig. 3. Immunohistochemistry for MMPs and TIMPs. Rabbit corneal frozen sections infected with *P. aeruginosa* were immunostained with mouse monoclonal antibodies against MMP-2 and MMP-9, TIMP-1 and TIMP-2, and were visualized using a diaminobenzidine (DAB) detection system. (A) MMP-2 staining 24 h p.i. (B) MMP-9 staining 24 h p.i. (C) double immunostaining of MMP-9 24 h p.i. (×1000). (D) TIMP-1 staining 24 h p.i. (E) TIMP-2 staining 24 h p.i. All negative control specimens did not show any staining. Peripheral corneal areas are shown in the figures (original magnification, ×400). Note that MMP-2 is present exclusively in keratocytes (black arrows), whereas MMP-9 is present in inflammatory cells like PMNs (grey arrows), and macrophages (white arrows), rather than in keratocytes.